Microbiota tryptophan metabolism induces aryl hydrocarbon receptor activation and improves alcohol-induced liver injury

Laura Wrzosek, Dragos Ciocan, Cindy Hugot, Madeleine Spatz, Margot Dupeux, Camille Houron, Vanessa Liévin-Le Moal, Virginie Puchois, Gladys Ferrere, Nicolas Trainel, et al.

Microbiota tryptophan metabolism induces aryl hydrocarbon receptor activation and improves alcohol-induced liver injury

Laura Wrzosek[1,2$], Dragos Ciocan[1,2,3$], Cindy Hugot[1,2], Madeleine Spatz[1,2], Margot Dupeux[1,2,4], Camille Houron[1,2], Vanessa Liévin-Le Moal[1,2], Virginie Puchois[1,2], Gladys Ferrere[1,2], Nicolas Trainel[1,2], Françoise Mercier-Nomé[5], Sylvère Durand[6], Guido Kroemer[7], Cosmin Sebastian Voican[1,2,3], Patrick Emond[8,9], Marjolene Straube[10], Harry Sokol[10,11,12], Gabriel Perlemuter[1,2,3*], and Anne-Marie Cassard[1,2*]

[$]These authors contributed equally to the work.

[*]Corresponding authors:

Anne-Marie Cassard : INSERM U996, 32 rue des carnets 92190 Clamart, France.

Tel: +33 1 41 28 80 37

Fax: +33 1 46 32 79 93

cassard.doulcier@u-psud.fr

Gabriel Perlemuter : INSERM U996, 32 rue des carnets, 92190 Clamart, France.

Tel: +33 1 41 28 80 37

Fax: +33 1 46 32 79 93

gabriel.perlemuter@aphp.fr.

[1]Université Paris-Saclay, Inserm U996, Inflammation, Microbiome and Immunosurveillance, 92140, Clamart, France.

[2]Institut Paris-Sud d'Innovation Thérapeutique (IPSIT), IFR141, Faculté de Pharmacie, Univ Paris-Sud, Université Paris-Saclay, Châtenay-Malabry, France. [3]AP-HP, Hepato-Gastroenterology and Nutrition, Hôpital Antoine-Béclère, Clamart, France. [4]AP-HP, Anatomie-Pathologique, Hôpital Kremlin-Bicêtre, le Kremlin-Bicêtre, France. [5]Université Paris-Saclay, Inserm, CNRS, Institut Paris Saclay d'Innovation thérapeutique, 92296, Châtenay-Malabry, France. [6]Metabolomics and Cell Biology Platforms, Gustave Roussy Cancer Campus, Villejuif, France. [7]Gustave Roussy Cancer Campus, Villejuif, France; INSERM, U1138, Paris, France; Equipe 11 labellisée par la Ligue Nationale contre le Cancer, Centre de Recherche des Cordeliers, Paris, France; Université Paris Descartes/Paris V, Sorbonne Paris Cité, Paris, France; Metabolomics and Cell Biology Platforms, Gustave Roussy Cancer Campus, Villejuif, France; Université Pierre et Marie Curie, Paris, France; Pôle de Biologie, Hôpital Européen Georges Pompidou, AP-HP, Paris, France; Karolinska Institute,

Department of Women's and Children's Health, Karolinska University Hospital, Stockholm, Sweden. [8]UMR 1253, iBrain, Université de Tours, Inserm, Tours, France. [9]CHRU de Tours, Service de Médecine Nucléaire In Vitro, Tours, France. [10]Sorbonne Université, Inserm, Centre de Recherche Saint-Antoine, CRSA, AP-HP, Hôpital Saint Antoine, Service de Gastroenterologie, F-75012 Paris, France. [11]Gastroenterology Department, Saint-Antoine Hospital, Assitance Publique-Hôpitaux de Paris (AP-HP), Paris, France. [12]INRA, UMR1319 Micalis, AgroParisTech, Jouy-en-Josas, France.

Electronic word count: 4052

Number of figures and tables: 5 figures

Keywords: alcoholic hepatitis, indole, fecal microbiota transplantation, human microbiota associated mice, fiber, pectin

ABSTRACT

Objective: Chronic alcohol consumption is an important cause of liver-related deaths. Specific intestinal microbiota profiles are associated with susceptibility or resistance to alcoholic liver disease in both mice and humans. We aimed to identify the mechanisms by which targeting intestinal microbiota can improve alcohol-induced liver lesions.

Design: We used human associated mice, a mouse model of alcoholic liver disease transplanted with the intestinal microbiota of alcoholic patients and used the prebiotic, pectin, to modulate the intestinal microbiota. Based on metabolomic analyses, we focused on microbiota tryptophan metabolites, which are ligands of the aryl hydrocarbon receptor (AhR). Involvement of the AhR pathway was assessed using both a pharmacological approach and AhR-deficient mice.

Results: Pectin treatment modified the microbiome and metabolome in human microbiota-associated alcohol-fed mice, leading to a specific fecal signature. High production of bacterial tryptophan metabolites was associated with an improvement of liver injury. The AhR agonist FICZ (6-formylindolo (3,2-b) carbazole) reduced liver lesions, similarly to prebiotic treatment. Conversely, inactivation of the *ahr* gene in alcohol-fed AhR *knock-out* mice abrogated the beneficial effects of the prebiotic. Importantly, patients with severe alcoholic hepatitis have low levels of bacterial tryptophan derivatives that are AhR agonists.

Conclusions: Improvement of alcoholic liver disease by targeting the intestinal microbiota involves the AhR pathway, which should be considered as a new therapeutic target.

SUMMARY BOX

What is already known about this subject?

● The intestinal microbiota is a causal factor of alcohol-induced liver lesions in mice and humans.

● Pectin is able to prevent alcohol-induced liver injury in mice by altering the intestinal microbiota.

● The protective effect of pectin is associated with an improvement of gut barrier function.

What are the new findings?

● Moderate amount of pectin can cure alcoholic liver disease in the context of the human microbiota.

● Pectin increases the production of tryptophan metabolites, which are aryl hydrocarbon receptor (AhR) ligands, by the microbiota, improving gut barrier function.

● Pharmacological activation of the AhR by FICZ, an exogenous AhR ligand, is sufficient to simulate the effect of pectin.

● AhR deficiency abrogates the beneficial effect of pectin, demonstrating a major role for the AhR pathway in the protective effect of the intestinal microbiota.

How might it impact on clinical practice in the foreseeable future?

Therapeutic options in alcohol-induced liver injury are limited. Our results show that targeting intestinal microbiota using moderate amount of pectin can reverse alcohol-induced liver injury through the AhR pathway. Modifying intestinal microbiota to increase its production of AhR ligands or AhR ligand administration could be new therapeutic targets for alcoholic patients.

INTRODUCTION

Chronic alcohol consumption is a major cause of liver-related deaths [1]. Severe alcoholic hepatitis (sAH) is a life-threading form of alcoholic liver disease (ALD), with few therapeutic options [2]. Recent studies have shown that specific microbiota profiles are associated with susceptibility or resistance to alcohol-induced liver lesions in both mice and humans, opening new therapeutic options [3, 4, 5, 6]. Moreover, the production of cytolysin by *Enterococcus faecalis* has been specifically shown to be involved in ALD development in 30% of sAH patients and its eradication by phagotherapy improves liver injury in a mouse model of ALD [7, 8]. Aside from deleterious bacteria, it is also relevant to identify bacteria that can protect patients from developing alcohol-induced liver lesions and to understand the molecular mechanisms involved in such protective effects.

Several studies have reported that modulation of intestinal microbiota (IM) composition by fecal microbiota transfer [4, 5, 9] or treatment with *Akkermansia muciniphila* [10], *Roseburia intestinalis* [11], other probiotics, or fiber/prebiotics [12, 13] can improve liver injury in mouse models of ALD. Molecular mechanisms by which microbiota alterations can improve alcohol-induced liver lesions are poorly understood and involve changes in the gut barrier and bacterial metabolites.

Disruption of the gut barrier correlates with endotoxemia and the severity of ALD in humans and mice [4, 5, 14]. This disruption is associated with a decrease in the production of mucus and anti-microbial peptides and the disruption of tight junctions [15, 16, 17]. Modulation of the IM by fecal transfer, prebiotics, or probiotics restores a leaky gut [4, 6, 13, 15]. Moreover, changes in IM composition in patients with ALD induce modifications in microbiota-associated metabolites, including short chain fatty acids (SCFAs) and bile acids [12], and are involved in the severity of alcohol-induced liver injury [5, 18, 19]. Among microbiota-associated metabolites, tryptophan-derived indoles, produced by a large number of bacteria, including *Bacteroides,* are ligands of the aryl hydrocarbon receptor (AhR). AhR signaling improves the function of the intestinal barrier by increasing local expression of IL-22 [20, 21] and, consequently, increases expression of antimicrobial proteins [22]. Moreover, the abundance of Bacteroidetes and level of plasma tryptophan decrease after acute alcohol administration in humans, suggesting impaired tryptophan metabolism [23].

Here, we aimed to identify the mechanisms by which targeting the IM with a prebiotic can improve alcohol-induced liver lesions. We used human microbiota-associated mice (HMA), which were transplanted with the IM of patients with sAH, to work in the context of the human

microbiota. We used the prebiotic fiber, pectin, to alter the IM. We and others have already shown that pectin can modify the mouse IM and prevent ALD by improving the leaky gut-barrier. However, the molecular mechanisms involved in this process and the effects of pectin in the context of the human IM are still unknown [4, 6]. We now demonstrate that pectin reshapes the microbiome in the context of the human microbiota and not only prevents but also reverses alcohol-induced liver injury in mice. Metabolomic studies showed that changes in the microbiota composition also induced alterations in bacterial tryptophan metabolism, leading to the high production of indole derivatives, which activate the AhR. Pharmacological treatment of mice with an AhR agonist simulating the effect of pectin on the liver and reversed ALD, whereas inactivation of the *ahr* gene in knock-out mice abrogated the effects of the beneficial microbiota in alcohol-fed mice. The results observed in the humanized mice are also supported by a decreased level of AhR agonists in patients with sAH, suggesting that AhR may be a new therapeutic target in ALD.

MATERIAL AND METHODS

Mice. Female C57BL/6J mice (Janvier laboratory, Le Genest, France) were kept in humidity and temperature-controlled rooms, on a 12-hour light-dark cycle. Mice had access to a chow diet and water *ad libitum* before the study. Body weight and food intake were measured three times a week. All our experimental procedures were validated by the ethical committees and the French veterinary minister (2015052715405651_v2 (APAFIS#729) and 2017042314557080v1(APAFIS#4788).

Treatments. In all our experiments, pectin was given at D21, as a curative treatment, using an alternative Lieber DeCarli diet containing different concentrations of pectin from apple (0.4%, 1%, 2% and 6.5%, w /w, Sigma-Aldrich, Saint Quentin Fallavier, France). To treat mice by an AhR agonist, the 6-formylindolo (3,2-b)carbazole (Ficz; Sigma-Aldrich) was re-suspended in dimethyl sulfoxide (DMSO; Sigma-Aldrich), diluted in olive oil (Sigma-Aldrich) and administered intraperitoneally. Ficz (1 µg/mouse) treatment was injected three times during the last week when mice were exposed to the maximum dose of alcohol (5%) and until euthanization. Control mice received DMSO vehicle diluted in olive oil intraperitoneally alone for the Ficz treatment group.

Fecal microbiota transfer. Mice received feces from alcoholic patients with severe alcoholic hepatitis as previously described [5, 24]. Two set of independent experiments were performed, a first set with feces from two different patients (F_1 and F_2) and a second set with feces from one patient (F_3). Briefly, feces from human patients were recovered and immediately stored at 4°C in an anaerobiosis generator (Genbox, Biomérieux, Capronne, France) to favour the preservation of anaerobic bacteria. All samples were processed within 24 h. Feces were rapidly diluted 100-fold in Brain Heart Infusion (BHI, Becton Dickinson) supplemented with 0.5mg/ml L-cysteine (Sigma-Aldrich, St-Louis, MO, USA) and 20% skim milk (Becton Dickinson) (vol/vol) and stored in aliquots at -80°C. This ready-to-use fecal suspension was used for FMT to mice.

Mice were fasted 1 h and then subjected to bowel cleansing by oral-gastric gavage with PEG (polyethylene glycol, Macrogol 4000, Fortrans, Ipsen Pharma, France). Four hours later, mice received the human feces by oral gastric gavage (200 µl of resuspended feces prepared as described above). Mice were then allowed free access to food and water. FMT was repeated twice a week for four weeks. Bowel cleansing was only performed on day 1.

Patients. Two groups of patients were included in the study: patients with severe alcoholic hepatitis (sAH) and alcoholic patients without alcoholic hepatitis and without cirrhosis (noAH). All patients were admitted to the hepato-gastroenterology department of Antoine-Béclère University Hospital, Clamart, France. Alcoholic patients were eligible for inclusion if they had consumed at least 50 g of alcohol per day over the previous year, were negative for hepatitis B surface antigens, and seronegative for antibodies against hepatitis C virus (HCV). Exclusion criteria were gastrointestinal bleeding, bacterial infection, hepatocellular carcinoma or other carcinoma, acute pancreatitis, other severe associated disease, diabetes mellitus, dyslipidemia, presence of anti-HIV antibodies, and antibiotic or probiotic intake in the last 3 months. A standardized questionnaire was used, to collect information about alcohol consumption [25]. Severe alcoholic hepatitis was suspected in patients with a Maddrey score > 32 and was confirmed by a liver biopsy (histological score for AH ≥ 6 with neutrophilic infiltration)[26, 27]. Feces from 3 independent patients with severe alcoholic hepatitis were used for the fecal transfer in mice.

The study was carried out in accordance with the Helsinki Declaration and was approved by the Ile de France VII ethics committee (Bicêtre Hospital, 94270 le Kremlin-Bicêtre, France). All the participants provided written informed consent.

Statistical analyses. Results are represented as the mean ± SEM. Statistical comparison was performed by first testing the normality of the data using the Shapiro-Wilk test of normality and then performing unpaired Mann-Whitney, unpaired t-test, Kruskal-Wallis or ANOVA tests as appropriate (Graphpad Prism, Graphpad Software Inc, La Jolla, California, USA); $p < 0,05$ was considered to be statistically significant. $^{*}p < 0.05$, $^{**}p < 0.01$, $^{***}p < 0.001$.

See the Supplementary section for the sources of materials and detailed methods.

RESULTS

Altering the intestinal microbiota reverses alcohol-induced liver lesions

We tested whether altering the intestinal microbiota can reverse the progression of alcohol-induced liver lesions using human microbiota-associated mice (HMA) [24, 28]. We used HMA mice transplanted with the microbiota from sAH patients, as we have previously shown that the intestinal microbiota worsens alcohol-induced liver lesions in this model [5]. Pectin, a dietary fiber known to favor the growth of specific bacterial genera, such as

Bacteroides [4, 29], which are reduced by alcohol intake [27], was used to alter the intestinal microbiota. Conventional (Alc) and HMA mice from three independent patients with sAH (Alc F_1, Alc F_2, Alc F_3) were fed alcohol using the Lieber DeCarli (LDC) diet, as described previously [4] (**Fig. 1a**). The clinical characteristics of the donors with sAH are presented in **Supplementary Table 1**. Principal coordinate analysis (PCoA) showed that alcohol, human microbiota transfer, and pectin treatment induced changes in intestinal microbiota composition (unweighted Unifrac, ANOSIM, $r = 0.59$, $P < 0.001$, **Fig. 1b and Supplementary Fig. 1a, c**). These changes included an increase in the *Bacteroides* genus in the pectin-treated group (**Fig. 1c and Supplementary Fig. 1b, d**).

HMA alcohol-fed mice developed liver lesions during the first week of alcohol intake, as shown by liver TG accumulation and an increase in ALT levels and several markers of inflammation (**Supplementary Fig. 2 a-e**). At this point, mice were treated with pectin in order to alter intestinal microbiota. Pectin did not modify the alcohol absorption (**Fig 1a and Supplementary Fig. 2f**). Changing microbiota by using pectin, reversed alcohol-induced liver lesions in HMA mice fed alcohol. These mice (Alc F_1P) had lower levels of ALT (**Fig. 1d**), liver TG (**Fig. 1e**), steatosis (**Fig. 1f**), and liver inflammation markers (*ccl2*, *tnfα*, *il1β* and *ccl3*) (**Fig. 1g**) than Alc F_1 and Alc mice. We obtained similar modifications of the intestinal microbiota and recovery of alcohol-induced liver lesions in HMA mice using feces from two other independent sAH patients (Alc F_2 and Alc F_3, **Supplementary Fig. 3 and 4**).

Altering the intestinal microbiota using high-dose of fiber may be associated with poor tolerance (bloating, abdominal distension) [30]. We therefore tested the efficacy of lower doses of pectin on ALD. Two percent pectin induced similar changes of the alcohol-induced liver lesions and gut barrier function while improving treatment tolerance (**Supplementary Fig. 4**). Pectin treatment induced dose-dependent changes in the intestinal microbiota (**Supplementary Fig. 5a-d**). Among the specific changes observed in the LEfSe analysis, Alc F_3 P2 showed an increase in the abundance of the Bacteroidetes phylum, a decrease in the abundance of the Firmicutes phylum, and an increase in the abundance of *Bacteroides* and *Lactobacillus* genera, similar to that of Alc F_3 P6.5 relative to Alc F_3 (**Supplementary Fig. 5d)**. However, the increase in the abundance of Proteobacteria and Enterobacteriaceae observed in the Alc F_3 P6.5 mice was not observed in the Alc F_3 P2 mice (**Supplementary Fig. 5e**).

Altering the intestinal microbiota improves gut-barrier function in alcohol-fed human microbiota associated mice

Disruption of the intestinal barrier correlates with the severity of liver injury in ALD [4, 5, 6, 15, 31]. Alcohol-induced gut barrier disruption results in a decrease in the level of the antimicrobial peptides *reg3β* and *reg3γ* and mucus production [4, 6]. Restoration of these functions is required to improve alcohol-induced liver injury [4, 6, 16, 32]. Altering the intestinal microbiota improved liver injury through improvement of the gut barrier function, as shown by an increase in antimicrobial peptide (*reg3β* and *reg3γ*) mRNA levels in the colon and ileum, and the proportion of goblet cells (**Supplementary Fig. 6a-g**). This was associated with an improvement of intestinal permeability, as shown by an increase in tight junction proteins (*ZO-1* and *occludin*) as shown by mRNA levels and immunoflourescence in the colon and ileum (**Supplementary Fig. 6h-i and Supplementary Fig. 7**) and a decrease of bacterial translocation into the liver (**Supplementary Fig. 6j**). These results show that altering the microbiota improves the gut barrier and reverses alcohol-induced liver injury, despite on-going heavy alcohol consumption.

Altering the intestinal microbiota modifies its functions and the fecal metabolome

We next explored the functional impact of altering the intestinal microbiota using pectin by generating the predicted metagenome using Phylogenetic Investigation of Communities by Reconstruction of Unobserved States (PICRUSt) [33]. A total of 4,977 KEGG orthologs were assigned to 146 metabolic pathways and 115 structural complex modules. Pectin-treated mice showed a higher number of bacterial genes involved in carbohydrate, lipid, and amino-acid metabolism (**Fig. 2a**). Conversely, control mice showed a higher number of bacterial genes involved in amino-acid, energy, and cofactor and vitamin metabolism. We obtained similar predicted metagenome profiles in mice transplanted with the intestinal microbiota of the two other independent patients (F_2 and F_3) (**Supplementary Table 2**).

We further studied whether such changes in the bacterial pathways induce alterations in the fecal metabolome by performing targeted metabolomic profiling. PCA and heatmaps showed that altering the intestinal microbiota induced a specific fecal metabolomic profile (**Fig. 2b, c**). Enrichment analysis using Metabolom Analyst led to the identification of 52 pathways that were modified between Alc F_1 and Alc F_1 P mice (FDR < 0.05) (**Fig. 2d** and **Supplementary Table 3)**. These pathways belong to the metabolism of amino acids (lysine, tyrosine, tryptophan, valine, leucine, isoleucine, and beta-alanine), carbohydrates (starch and sucrose, pentose and glucose interconversion, and ascorbate) lipids, and vitamins (biotin and ascorbate). Many of the changes in the fecal metabolomic pathways belong to those highlighted

by the predicted bacterial metagenome (**Fig. 2a, d**). These results were also confirmed when using lower doses of pectin (**Supplementary Fig. 8**).

Among the amino acids of which the levels were modified by pectin, we specifically identified a decrease in the levels of tryptophan and indole, precursors of microbiota-derived tryptophan metabolites (**Fig. 2e**). We then performed specific metabolomic profiling of tryptophan metabolites, as we observed an increase in the abundance of *Bacteroides*, taxa that can metabolize tryptophan into indole derivatives, in pectin-treated mice. We observed a decreased level of indole-3-acrylic acid in alcohol-fed conventional and HMA mice as compared to control mice and a decrease in overall AhR agonists (sum of 3-indoxyl sulfuric acid, 5-Methoxy-3-indoleacetic acid, indole-3-acetic acid, indole-3-acrylic acid, indole-3-aldehyde, indole-3-lactic acid, indole-3-propionic acid) in alcohol-fed HMA mice. These changes were restored after pectin treatment with an overall increase in total AhR agonists in pectin treated mice (**Fig. 2f**).

Activation of the AhR pathway improves alcohol-induced liver injury

Altering the intestinal microbiota with pectin in the HMA mouse model of ALD reverses alcohol-induced injury and is associated with changes in the microbiota and tryptophan metabolism. We therefore studied the role of the AhR pathway, which can be activated by bacterial tryptophan metabolites. We analyzed the expression of *cyp1a1* and its repressor *ahrr*, target genes of AhR activation in the colon. Their expression in the colon (**Fig. 3a**), together with that of *il22* [20] and *il17* (**Fig. 3b**), which are also controlled by AhR activation [34], increased after altering the intestinal microbiota by pectin treatment. We then assessed the direct involvement of AhR in the improvement of alcohol-induced injury by treating mice with an AhR agonist, 6-formylindolo (3,2-b) carbazole (Ficz). Treatment of Alc mice with Ficz increased the expression of AhR target genes *Cyp1a1* and *Scd1* in the liver (**Fig. 3c**) and decreased alcohol-induced liver lesions, with a decrease in ALT, liver TG, and inflammatory marker levels (**Fig. 3d, e**). Treatment with Ficz also increased antimicrobial peptide levels in the colon and ileum (**Fig. 3f, g**) but only the expression of *Reg3γ* in the ileum reached statistical significance, simulating the effects of pectin. We next tested whether AhR signaling mediates the effects of pectin using alcohol-fed mice deficient for AhR (AhR KO). Although pectin treatment still restored ALT levels in alcohol-fed AhR KO mice, it could neither alleviate steatosis (**Fig. 4a, b**) nor restore *cyp1a1* and *ahrr* mRNA levels (**Fig. 4c**). Accordingly, restoration of *il22*, *reg3β*, and *reg3γ* mRNA levels by pectin treatment was also abrogated (**Fig.**

4d). Overall, these data show that the effects of pectin are, at least partially, mediated by AhR pathways.

Tryptophan metabolism is impaired in patients with severe alcoholic hepatitis

We next explored the relevance of impaired tryptophan metabolism in the context of human disease and analyzed fecal and serum samples of alcoholic patients with (sAH) or without alcoholic hepatitis (noAH) (**Supplementary Table 4**). There were no differences in the fecal levels of tryptophan, kynurenine, or AhR agonists between alcoholic patients, regardless of the severity of the liver injury (noAH or sAH) (data not shown). There was also no difference in the serum level of kynurenine between alcoholic patients (**Fig. 5a**). Conversely, serum levels of tryptophan and AhR agonists were lower in sAH patients than in noAH patients (**Fig. 5a**). We also found negative correlations between serum levels of Trp and AST ($r = -0.6$, $p < 0.01$), bilirubin ($r = -0.7$, $p < 0.001$), prothrombin time ($r = -0.7$, $p < 0.001$), and MELD score ($r = -0.6$, $p < 0.001$) (**Fig. 5b**). This suggest that tryptophan metabolism is impaired in patients with alcoholic hepatitis and that the modulation of AhR could be a new therapeutic target.

DISCUSSION

The IM plays a role in the pathophysiology of ALD and bacterial composition contributes to the severity of liver injury, independently of alcohol intake [2, 5]. Bacteria interact directly with the host and indirectly through a large panel of bacterial metabolites [35]. Impairment of several bacterial metabolic functions has been shown to exacerbate ALD, including that of bacterial synthesis of saturated long-chain fatty acids [36], bile acids [5, 19, 27], and tryptophan [37]. In ALD, disruption of the intestinal barrier correlates with the severity of liver lesions [4, 15, 31]. The role of the IM in the development of a leaky gut is associated with decreased levels of antimicrobial Reg 3 peptides and decreased mucus production [4, 16]. Altering the IM using probiotics or prebiotics in murine models can prevent ALD by modulating these functions [6, 10, 38, 39, 40]. Specifically, pectin, a fiber that modulates the intestinal microbiota, can prevent alcohol-induced liver injury by improving gut barrier function [4]. Nevertheless, a preventive effect of such a treatment is not relevant for patients with alcohol-use disorders that have ALD. Therefore, we addressed the effect of pectin in a mouse model of ongoing alcohol administration after the onset of liver injury. We focused on bacterial indole derivatives, as the molecular mechanisms by which fiber-induced changes of the IM improve ALD have not been elucidated.

Here, we show that pectin, used as a curative treatment, is able to reverse alcohol-induced liver injury in the context of the human microbiota. We used HMA transplanted with the feces of alcoholic patients with sAH. Liver injury in these mice is worse than that of wildtype alcohol-fed mice. Improvement of liver lesions is associated with improved gut barrier function, including the restoration of mucus production and antimicrobial Reg 3 peptide levels. Pectin, as a dietary fiber, is known to favor the growth of specific bacterial genera, such as *Bacteroides* [4, 29]. In alcoholic patients, sAH is associated with a decrease in the abundance of Bacteroidetes and changes in IM function [5, 41]. A similar decrease in the abundance of Bacteroidetes has also been observed in animal models of ALD [4]. Here, we show that pectin induces an increase in the abundance of *Bacteroides*, regardless of the effective dose.

A high dose of pectin (6.5%) was also associated with an increased abundance of Proteobacteria, which could pose safety concerns, as several species of this phylum are considered to be opportunistic pathogens [42]. Moreover, fermentable fiber (including pectin) has been reported to induce an increase in the abundance of Proteobacteria and hepatocarcinoma in several animal models (TLR5, TLR4, and Lcn2 –deficient mice). This is due to the inability of the innate immunity in the gut to prevent the translocation of Proteobacteria species [43]. However, in our study, the lower dose of pectin (2%) used to improve intestinal tolerance to a

diet rich in fiber abrogated Proteobacteria overgrowth and achieved the beneficial effects that we observed on alcohol-induced liver lesions with a pectin-enriched diet. The amount of pectin to administrate in patients to match the minimal effective dose described in our study (2%) would be of 40 g/day. Of note, the recommended daily dose of fiber intake ranges between 30-38 g/day in men and 21-25 g/day in women [44]. Nevertheless, the amount of fiber consumed by humans is dependent on their diet. It has been suggested that omnivores consumed less than 23 g of fibers/day, vegetarians significantly more (37 g/day) and vegans the most (47 g/day) [45]. Patients with chronic liver disease (viral and alcoholic cirrhosis) have a lower intake of vegetables which are rich in fibers [46]. Moreover, a high-fiber diet has been related to regression of NAFLD [47] and recent epidemiological data showed that dietary fiber intake, especially soluble fibers (such as pectin), is inversely associated with the risk of several chronic diseases and with mortality [48]. Studies investigating pectin administration in different conditions used up to 60 g/day and reported good tolerance [49]. The main side effect was bloating but individual sensitivity to develop side effects is highly variable [50]. These data suggest that a moderate amount of pectin may be a promising and safe alimentary complement in the management of alcoholic patients.

We further analyzed intestinal metabolites to investigate the mechanisms by which pectin-induced modifications of the IM reduce alcohol-induced gut and liver injuries. The microbiota reshaped by pectin harbored more genes involved in amino-acid and xenobiotic metabolism. This metagenomic prediction was confirmed by the quantification of fecal metabolites. We specifically identified a decrease in tryptophan levels and an increase in the level of indole derivatives. These metabolites are only produced by the intestinal microbiota from tryptophan [37]. Several microbiota-derived tryptophan metabolites are able to activate the AhR, thus playing a key role in gut homeostasis through the regulation of anti-microbial peptide and mucus production by IL-22 [21]. Moreover, it has been previously shown that IL-22 is down-regulated in alcohol-fed mice and oral treatment with recombinant IL-22 or bacteria that produce this cytokine prevents alcohol-induced liver injury [37, 51]. AhR activation has been shown to improve inflammatory bowel disease [52] and metabolic syndrome [37, 53, 54]. Moreover, hepatic AhR activation prevents HSC activation and the expression of genes required for liver fibrogenesis by disrupting the interaction of Smad3 with β-catenin [55]. Here, we show that the improvement of mucus and antimicrobial peptide production by pectin is associated with the restoration of AhR-responsive gene expression, including that of IL-22, Cyp1a1, and ahrr. Conversely, low levels of *reg3β*, *reg3γ*, and mucus production in untreated alcohol-fed mice correlated with lower levels of *il22*, Cyp1a1, and ahrr.

We also treated mice with an AhR agonist, FICZ, to address the direct involvement of AhR in the effects of pectin. FICZ treatment was sufficient to mediate a reduction in alcohol-induced injury. In contrast, pectin treatment of AhR-deficient alcohol-fed mice had only a minimal effect on alcohol-induced liver lesions suggesting that the effects of pectin treatment in our model of ALD are not solely medicated by AhR. Indeed, pectin induces broad changes at the microbial and metabolomic level and other mechanisms independent of AhR could also mediate the effect observed in our study.

The relevance of impaired tryptophan metabolism in the context of human disease was confirmed by reduced serum levels of tryptophan and AhR agonists in patients with sAH. Conversely, there were no differences in the fecal levels of tryptophan, kynurenine, or AhR agonists between alcoholic patients, regardless of the severity of the liver injury (noAH or sAH). However, it has been reported that patients with alcoholic hepatitis have lower levels of fecal indole-3-acetic acid and indole-3-lactic acid than healthy patients who do not consume alcohol [37]. These discrepancies suggest that alcohol induces impairment of tryptophan metabolism independently of liver disease.

Our results provide the basis for further studies in patients with ALD that will aim to correct the AhR-ligand deficiency. Indeed, it has been recently shown that *Lactobacillus reuteri*, which is known to produce AhR agonists, improves ALD [37], as well as treatment with a direct agonist, such as indole-3 acetic acid. Moreover, treatment with *Lactobacillus reuteri* can also improve metabolic syndrome [53] and colitis [56, 57] in animal models. Indole-3-pyruvic acid, an AhR agonist, improves experimental colitis [58] and indigo, a tryptophan metabolite that activates the AhR, is effective in inducing remission in patients with ulcerative colitis [59].

In conclusion, our study shows that alcohol-induced liver lesions can be reversed by modifying AhR-agonist production by the IM. As there is no treatment that can reverse alcohol-induced liver lesions other than liver transplant, modulation of the AhR pathways by supplementation with prebiotics, AhR ligand-producing bacteria, or pharmacological AhR ligands, may hold promise in the development of new therapeutic approaches to ALD.

Acknowledgments. The authors thank Mylène Levant, Baptiste Lecomte, and Sarah Mendez for follow-up of the mice, the Plaimmo Platform, PHIC platform (Morgan Ocimek and Séverine Domenichini), and Nicolas Sorhaindo for plasma quantification (Plateforme de Biochimie, Bichat). We also thank the NED team (Olivier Zemb and Béatrice Gabinaud) and the GeT-PlaGe platform for their help with the sequencing data.

Disclosures: DC received travel funds from Biocodex and Gilead, lecture fees from Gilead, and royalties from John Libbey Eurotext. HS received unrestricted study grants from Danone, Biocodex, and Enterome and board membership, consultancy, or lecture fees from Carenity, Abbvie, Astellas, Danone, Ferring, Mayoly Spindler, MSD, Novartis, Roche, Tillots, Enterome, Maat, BiomX, Biose, Novartis, and Takeda and is a co-founder of Exeliom Biosciences. GP received travel funds from Janssen and Gilead, consulting fees from Bayer, Biocodex, Roche, Gilead, Pierre Fabre, and Servier, and royalties from Elsevier-Masson, Solar, Flammation/Versilio, and John Libbey Eurotext. AMC received travel funds and consulting fees from Biocodex and royalties from Elsevier-Masson, Solar, Flammation/Versilio, and John Libbey Eurotext. All other authors declare no conflicts of interest.

Financial support: This work was supported by INSERM, Université Paris-Sud, "Fondation pour la recherche médicale" (FRM), the National French Society of Gastroenterology (SNFGE), "Association Française pour l'Etude du Foie" (AFEF), "Fondation pour la Recherche en Alcoologie" (FRA/IREB), "Institut de Recherches Internationales Servier" (IRIS), and "Groupement transversal INSERM sur le microbiote" (GPT microbiota). DC received a grant from Biocodex. MSp received a grant from the Laboratory of Excellence LERMIT supported by the "Agence Nationale de la Recherche" (ANR-10-LABX-33). MD received a grant from FRM. CHo received a CIFRE (Conventions Industrielles de Formation par la Recherche) scholarship in collaboration with the IRIS. HS received funding from the European Research Council (ERC) under the European Union's Horizon 2020 Research and Innovation Programme (ERC-2016-StG-71577).

Authors' Contributions: LW and DC: contributed equally to this work for the study concept and design, acquisition, analysis, and interpretation of data, and drafting of the manuscript. CHu, MSp, CHo, VLLM, VP, GF, NT and MSt: technical support. MD and FMN: histological analysis. SD and GK: fecal metabolite quantification. CSV: provided patients. HS: provided

AhR KO mice. HS and PE: tryptophan metabolite analysis. GP: critical revision of the manuscript, obtained funding, and provided patients. AMC: study concept, design, and supervision, analysis and interpretation of the data, drafting of the manuscript, and funding raising.

REFERENCES

1 Collaborators GBDA. Alcohol use and burden for 195 countries and territories, 1990-2016: a systematic analysis for the Global Burden of Disease Study 2016. Lancet 2018;**392**:1015-35.

2 Seitz HK, Bataller R, Cortez-Pinto H, Gao B, Gual A, Lackner C*, et al.* Alcoholic liver disease. Nat Rev Dis Primers 2018;**4**:16.

3 Chen Y, Yang F, Lu H, Wang B, Lei D, Wang Y*, et al.* Characterization of fecal microbial communities in patients with liver cirrhosis. Hepatology 2011;**54**:562-72.

4 Ferrere G, Wrzosek L, Cailleux F, Turpin W, Puchois V, Spatz M*, et al.* Fecal microbiota manipulation prevents dysbiosis and alcohol-induced liver injury in mice. J Hepatol 2017;**66**:806-15.

5 Llopis M, Cassard AM, Wrzosek L, Boschat L, Bruneau A, Ferrere G*, et al.* Intestinal microbiota contributes to individual susceptibility to alcoholic liver disease. Gut 2016;**65**:830-9.

6 Yan AW, Fouts DE, Brandl J, Starkel P, Torralba M, Schott E*, et al.* Enteric dysbiosis associated with a mouse model of alcoholic liver disease. Hepatology 2011;**53**:96-105.

7 Duan Y, Llorente C, Lang S, Brandl K, Chu H, Jiang L*, et al.* Bacteriophage targeting of gut bacterium attenuates alcoholic liver disease. Nature 2019;**575**:505-11.

8 Llorente C, Jepsen P, Inamine T, Wang L, Bluemel S, Wang HJ*, et al.* Gastric acid suppression promotes alcoholic liver disease by inducing overgrowth of intestinal Enterococcus. Nat Commun 2017;**8**:837.

9 Philips CA, Pande A, Shasthry SM, Jamwal KD, Khillan V, Chandel SS*, et al.* Healthy Donor Fecal Microbiota Transplantation in Steroid-Ineligible Severe Alcoholic Hepatitis: A Pilot Study. Clin Gastroenterol Hepatol 2017;**15**:600-2.

10 Grander C, Adolph TE, Wieser V, Lowe P, Wrzosek L, Gyongyosi B*, et al.* Recovery of ethanol-induced Akkermansia muciniphila depletion ameliorates alcoholic liver disease. Gut 2017.

11 Seo B, Jeon K, Moon S, Lee K, Kim WK, Jeong H*, et al.* Roseburia spp. Abundance Associates with Alcohol Consumption in Humans and Its Administration Ameliorates Alcoholic Fatty Liver in Mice. Cell Host Microbe 2020;**27**:25-40 e6.

12 Bajaj JS. Alcohol, liver disease and the gut microbiota. Nat Rev Gastroenterol Hepatol 2019;**16**:235-46.

13 Cassard AM, Ciocan D. Microbiota, a key player in alcoholic liver disease. Clin Mol Hepatol 2018;**24**:100-7.

14 Rao R. Endotoxemia and gut barrier dysfunction in alcoholic liver disease. Hepatology 2009;**50**:638-44.

15 Chen P, Starkel P, Turner JR, Ho SB, Schnabl B. Dysbiosis-induced intestinal inflammation activates TNFRI and mediates alcoholic liver disease in mice. Hepatology 2015;**61**:883-94.

16 Hartmann P, Chen P, Wang HJ, Wang L, McCole DF, Brandl K*, et al.* Deficiency of intestinal mucin-2 ameliorates experimental alcoholic liver disease in mice. Hepatology 2013;**58**:108-19.

17 Yoseph BP, Breed E, Overgaard CE, Ward CJ, Liang Z, Wagener ME*, et al.* Chronic alcohol ingestion increases mortality and organ injury in a murine model of septic peritonitis. PLoS One 2013;**8**:e62792.

18 Bajaj JS, Hylemon PB. Gut-liver axis alterations in alcoholic liver disease: Are bile acids the answer? Hepatology 2018;**67**:2074-5.

19 Hartmann P, Hochrath K, Horvath A, Chen P, Seebauer CT, Llorente C*, et al.* Modulation of the intestinal bile acid/farnesoid X receptor/fibroblast growth factor 15 axis improves alcoholic liver disease in mice. Hepatology 2018;**67**:2150-66.

20 Lee JS, Cella M, McDonald KG, Garlanda C, Kennedy GD, Nukaya M*, et al.* AHR drives the development of gut ILC22 cells and postnatal lymphoid tissues via pathways dependent on and independent of Notch. Nat Immunol 2011;**13**:144-51.
21 Zelante T, Iannitti RG, Cunha C, De Luca A, Giovannini G, Pieraccini G*, et al.* Tryptophan catabolites from microbiota engage aryl hydrocarbon receptor and balance mucosal reactivity via interleukin-22. Immunity 2013;**39**:372-85.
22 Zheng Y, Valdez PA, Danilenko DM, Hu Y, Sa SM, Gong Q*, et al.* Interleukin-22 mediates early host defense against attaching and effacing bacterial pathogens. Nat Med 2008;**14**:282-9.
23 Badawy AA, Morgan CJ, Lovett JW, Bradley DM, Thomas R. Decrease in circulating tryptophan availability to the brain after acute ethanol consumption by normal volunteers: implications for alcohol-induced aggressive behaviour and depression. Pharmacopsychiatry 1995;**28 Suppl 2**:93-7.
24 Wrzosek L, Ciocan D, Borentain P, Spatz M, Puchois V, Hugot C*, et al.* Transplantation of human microbiota into conventional mice durably reshapes the gut microbiota. Sci Rep 2018;**8**:6854.
25 Williams GD, Proudfit AH, Quinn EA, Campbell KE. Variations in quantity-frequency measures of alcohol consumption from a general population survey. Addiction 1994;**89**:413-20.
26 Alcoholic liver disease: morphological manifestations. Review by an international group. Lancet 1981;**1**:707-11.
27 Ciocan D, Voican CS, Wrzosek L, Hugot C, Rainteau D, Humbert L*, et al.* Bile acid homeostasis and intestinal dysbiosis in alcoholic hepatitis. Aliment Pharmacol Ther 2018.
28 Le Roy T, Debedat J, Marquet F, Da-Cunha C, Ichou F, Guerre-Millo M*, et al.* Comparative Evaluation of Microbiota Engraftment Following Fecal Microbiota Transfer in Mice Models: Age, Kinetic and Microbial Status Matter. Front Microbiol 2018;**9**:3289.
29 Dongowski G, Lorenz A, Proll J. The degree of methylation influences the degradation of pectin in the intestinal tract of rats and in vitro. The Journal of nutrition 2002;**132**:1935-44.
30 Cummings JH, Macfarlane GT, Englyst HN. Prebiotic digestion and fermentation. Am J Clin Nutr 2001;**73**:415S-20S.
31 Mathurin P, Deng QG, Keshavarzian A, Choudhary S, Holmes EW, Tsukamoto H. Exacerbation of alcoholic liver injury by enteral endotoxin in rats. Hepatology 2000;**32**:1008-17.
32 Wang L, Fouts DE, Starkel P, Hartmann P, Chen P, Llorente C*, et al.* Intestinal REG3 Lectins Protect against Alcoholic Steatohepatitis by Reducing Mucosa-Associated Microbiota and Preventing Bacterial Translocation. Cell Host Microbe 2016;**19**:227-39.
33 Langille MG, Zaneveld J, Caporaso JG, McDonald D, Knights D, Reyes JA*, et al.* Predictive functional profiling of microbial communities using 16S rRNA marker gene sequences. Nat Biotechnol 2013;**31**:814-21.
34 Hayes MD, Ovcinnikovs V, Smith AG, Kimber I, Dearman RJ. The aryl hydrocarbon receptor: differential contribution to T helper 17 and T cytotoxic 17 cell development. PLoS One 2014;**9**:e106955.
35 Postler TS, Ghosh S. Understanding the Holobiont: How Microbial Metabolites Affect Human Health and Shape the Immune System. Cell Metab 2017;**26**:110-30.
36 Chen P, Torralba M, Tan J, Embree M, Zengler K, Starkel P*, et al.* Supplementation of Saturated Long-Chain Fatty Acids Maintains Intestinal Eubiosis and Reduces Ethanol-induced Liver Injury in Mice. Gastroenterology 2015;**148**:203-14 e16.
37 Hendrikx T, Duan Y, Wang Y, Oh JH, Alexander LM, Huang W*, et al.* Bacteria engineered to produce IL-22 in intestine induce expression of REG3G to reduce ethanol-induced liver disease in mice. Gut 2018.

38 Bull-Otterson L, Feng W, Kirpich I, Wang Y, Qin X, Liu Y*, et al.* Metagenomic analyses of alcohol induced pathogenic alterations in the intestinal microbiome and the effect of Lactobacillus rhamnosus GG treatment. PLoS One 2013;**8**:e53028.
39 Chen RC, Xu LM, Du SJ, Huang SS, Wu H, Dong JJ*, et al.* Lactobacillus rhamnosus GG supernatant promotes intestinal barrier function, balances Treg and TH17 cells and ameliorates hepatic injury in a mouse model of chronic-binge alcohol feeding. Toxicol Lett 2016;**241**:103-10.
40 Wang Y, Liu Y, Kirpich I, Ma Z, Wang C, Zhang M*, et al.* Lactobacillus rhamnosus GG reduces hepatic TNFalpha production and inflammation in chronic alcohol-induced liver injury. J Nutr Biochem 2013;**24**:1609-15.
41 Ciocan D, Rebours V, Voican CS, Wrzosek L, Puchois V, Cassard AM*, et al.* Characterization of intestinal microbiota in alcoholic patients with and without alcoholic hepatitis or chronic alcoholic pancreatitis. Sci Rep 2018;**8**:4822.
42 Shin NR, Whon TW, Bae JW. Proteobacteria: microbial signature of dysbiosis in gut microbiota. Trends Biotechnol 2015;**33**:496-503.
43 Singh V, Yeoh BS, Chassaing B, Xiao X, Saha P, Aguilera Olvera R*, et al.* Dysregulated Microbial Fermentation of Soluble Fiber Induces Cholestatic Liver Cancer. Cell 2018;**175**:679-94 e22.
44 Medicine Institute. Dietary Reference Intakes for Energy, Carbohydrate, Fiber, Fat, Fatty Acids, Cholesterol, Protein, and Amino Acids. 2005.
45 Davies GJ, Crowder M, Dickerson JW. Dietary fibre intakes of individuals with different eating patterns. Hum Nutr Appl Nutr 1985;**39**:139-48.
46 Buscail C, Bourcier V, Fezeu LK, Roulot D, Brule S, Ben-Abdesselam Z*, et al.* Eating Patterns in Patients with Compensated Cirrhosis: A Case-Control Study. Nutrients 2018;**10**.
47 Alferink LJM, Erler NS, de Knegt RJ, Janssen HLA, Metselaar HJ, Darwish Murad S*, et al.* Adherence to a plant-based, high-fibre dietary pattern is related to regression of non-alcoholic fatty liver disease in an elderly population. Eur J Epidemiol 2020.
48 Partula V, Deschasaux M, Druesne-Pecollo N, Latino-Martel P, Desmetz E, Chazelas E*, et al.* Associations between consumption of dietary fibers and the risk of cardiovascular diseases, cancers, type 2 diabetes, and mortality in the prospective NutriNet-Sante cohort. Am J Clin Nutr 2020;**112**:195-207.
49 Seyrig JA, Naveau S, Gonzales R, Petit R. Pectines. Gastroenterol Clin Biol 1983;**7**:1031-37.
50 Ralphs DNL, Lawaetz NJG. Effect of dietary fibre on gastric emptying in dumpers. Gut 1978;**19**:986-87.
51 Ki SH, Park O, Zheng M, Morales-Ibanez O, Kolls JK, Bataller R*, et al.* Interleukin-22 treatment ameliorates alcoholic liver injury in a murine model of chronic-binge ethanol feeding: role of signal transducer and activator of transcription 3. Hepatology 2010;**52**:1291-300.
52 Lamas B, Richard ML, Leducq V, Pham HP, Michel ML, Da Costa G*, et al.* CARD9 impacts colitis by altering gut microbiota metabolism of tryptophan into aryl hydrocarbon receptor ligands. Nat Med 2016;**22**:598-605.
53 Natividad JM, Agus A, Planchais J, Lamas B, Jarry AC, Martin R*, et al.* Impaired Aryl Hydrocarbon Receptor Ligand Production by the Gut Microbiota Is a Key Factor in Metabolic Syndrome. Cell Metab 2018.
54 Wang X, Ota N, Manzanillo P, Kates L, Zavala-Solorio J, Eidenschenk C*, et al.* Interleukin-22 alleviates metabolic disorders and restores mucosal immunity in diabetes. Nature 2014;**514**:237-41.
55 Yan J, Tung HC, Li S, Niu Y, Garbacz WG, Lu P*, et al.* Aryl Hydrocarbon Receptor Signaling Prevents Activation of Hepatic Stellate Cells and Liver Fibrogenesis in Mice. Gastroenterology 2019.

56 Mackos AR, Galley JD, Eubank TD, Easterling RS, Parry NM, Fox JG*, et al.* Social stress-enhanced severity of Citrobacter rodentium-induced colitis is CCL2-dependent and attenuated by probiotic Lactobacillus reuteri. Mucosal Immunol 2016;**9**:515-26.
57 Ahl D, Liu H, Schreiber O, Roos S, Phillipson M, Holm L. Lactobacillus reuteri increases mucus thickness and ameliorates dextran sulphate sodium-induced colitis in mice. Acta Physiol (Oxf) 2016;**217**:300-10.
58 Aoki R, Aoki-Yoshida A, Suzuki C, Takayama Y. Indole-3-Pyruvic Acid, an Aryl Hydrocarbon Receptor Activator, Suppresses Experimental Colitis in Mice. J Immunol 2018;**201**:3683-93.
59 Naganuma M. Treatment with indigo naturalis for inflammatory bowel disease and other immune diseases. Immunol Med 2019:1-6.

FIGURE LEGENDS

Figure 1. Altering the intestinal microbiota using pectin reverses alcohol induced liver lesions. Alc, alcohol-fed mice; Ctrl, control-fed mice; Alc F_1, alcohol-fed mice humanized with the microbiota from a patient with severe alcoholic hepatitis (sAH, patient F_1); Alc F_1 P, alcohol-fed mice humanized with microbiota from a patient with sAH (patient F_1) and treated with 6.5% pectin. (**a**) Experimental design: mice were progressively adapted to a semi-liquid, Lieber DeCarli (LDC) diet, then an ethanol diet (1-3%), and finally fed a 5% ethanol diet for one week. Pectin was introduced in the diet at the same time as the 5% ethanol. Microbiota analysis: (**b**) PCoA plot, showing the unweighted UniFrac distance ($p < 0.001$, $R = 0.58$, ANOSIM test, 10,000 permutations, using the first 5 PC); (**c**) LDA effect size (LEfSe) cladograms showing the taxa most differentially associated with Alc F_1 (red) or Alc F_1 P mice (yellow) (Wilcoxon rank-sum test). Circle sizes in the cladogram plot are proportional to bacterial abundance. The circles represent, going from the inner to outer circle: phyla, genus, class, order, and family. (**d**) ALT level in Ctrl (n = 8), Alc (n = 8), Alc F_1 (n = 12), and Alc F_1P (n = 10) mice. (**e**) Liver triglyceride quantification in Ctrl (n = 8), Alc (n = 8), Alc F_1 (n = 12), and Alc F_1P (n = 10) mice. (**f**) Representative images of liver sections stained with hematoxylin-eosin, scale bar 100 μm. (**g**) Liver mRNA levels determined by qPCR: *ccl2*, *tnfα*, *il1β*, and *ccl3* normalized to that of the *gapdh* gene in Ctrl (n = 4), Alc (n = 5), Alc F_1 (n = 12), and Alc F_1P (n = 10) mice. Results (d-g) are shown as the mean ± SEM. Significant results for $*p < 0.05$, $**p < 0.01$, and $***p < 0.001$ were determined by Mann-Whitney tests unless stated otherwise.

Figure 2. Functions of the intestinal microbiota and fecal metabolome are modified by pectin treatment. Ctrl, control-fed mice; Alc, alcohol-fed mice; Alc F_1 and Alc F_3, alcohol-fed mice humanized with microbiota from a patient with sAH (patients F_1 or F_3); Alc F_1P and Alc F_3P, alcohol-fed mice humanized with microbiota from a patient with sAH (patients F_1 or F_3) and treated with 6.5% pectin (F_1) or 2% pectin (F_3). (**a**) LEfSe cladograms of KEGG pathway contributions of predicted metagenomic data in Alc F_1 and Alc F_1P mice (Wilcoxon rank-sum test). In **a**: Ctrl n = 8, Alc n = 10, Alc F_1 n = 14, and Alc F_1P n = 10 mice per experiment. (**b**) PCA ordination plot on all fecal metabolomic data (147 metabolites). (**c**) Heatmap showing the first 60 metabolites ranked by t-tests between Alc F_1 (red) and Alc F_1P (green). (**d**) Metabolic enrichment analysis showing the most altered pathways in Alc F_1P mice relative to Alc F_1 mice. All matched pathways are displayed as circles. The color and size of each circle are based on the p value and pathway impact value, respectively. The graph was obtained by plotting the

−log of p values from the pathway enrichment analysis on the y axis and the pathway impact values, derived from the pathway topology analysis, on the x axis. (**e**) Relative fecal levels of tryptophan, kynurenine, and indole. In **b-e**: Ctrl n = 8, Alc n = 10, Alc F_1 n = 11, and Alc F_1P n = 7 mice per group. (**f**) Tryptophan metabolites quantification in faeces. Aryl hydrocarbon receptor (AhR) ligands (methyl-indole 3-acetic acid, indole 3-propionic acid, indole 3-aldehyde, indole 3-acrylic acid, and 3-indoxyl sulfuric acid). In **f**: Ctrl n = 8, Alc n = 9, Alc F_3 n = 6, and Alc F_3P n = 8 mice per group. *p < 0.05, **p<0.01, ***p<0.001 by the ANOVA or Kruskal-Wallis test with Tukey or Dunn correction for multiple comparisons, as appropriated.

Figure 3. AhR activation reverses alcohol-induced liver lesions. Ctrl, control-fed mice; Alc, alcohol-fed mice. (**a,b**) Alc F_3, alcohol-fed mice humanized with the microbiota from a patient with sAH (patient F_3); Alc F_3 P2, Alc F_3 P6.5, alcohol-fed mice humanized with the microbiota from a patient with sAH (patient F_3) and treated with 2 or 6.5% pectin. Colon mRNA levels were determined by qPCR: (**a**) *cyp1a1* and *ahrr,* (**b**) *il17* and *il22*, normalized to that of the *18s* gene, in Ctrl (n = 7), Alc (n = 8), Alc F_3 (n = 4), Alc F_3 P2 (n = 15), and Alc F_3 P6.5 (n = 16) mice. (**c-g**) DMSO or Ficz, mice treated with DMSO or Ficz. (**c**) Liver *cyp1a1* and *scd1*, normalized to that of the *gapdh* gene. (**d**) ALT level and liver triglyceride quantification in Ctrl DMSO (n = 7), Alc DMSO (n = 12), Ctrl Ficz (n = 8), and Alc Ficz (n = 8) mice. (**e**) Liver mRNA levels determined by qPCR: *ccl2* and *tnfα*, normalized to that of the *gapdh* gene, in Ctrl DMSO (n = 6), Alc DMSO (n = 11), Ctrl Ficz (n = 8), and Alc Ficz (n = 7) mice. (**f**) Colon mRNA levels determined by qPCR: *reg3β* and *reg3γ*, normalized to that of the *gapdh* gene. **(g)** Ileum mRNA levels determined by qPCR: *reg3β* and *reg3γ*, normalized to that of the *gapdh* gene, in Ctrl DMSO (n = 8), Alc DMSO (n = 12), Ctrl Ficz (n = 8), and Alc Ficz (n = 10) mice.

Figure 4. KO of AhR partly blocks the liver protective effects of pectin.
(**a-d**) WT, wild type mice; AhR KO, AhR deficient mice; Alc P2, alcohol-fed mice treated with 2% pectin. (**a**) ALT levels and liver triglyceride quantification in WT Ctrl (n = 8), WT Alc (n = 5), WT Alc P (n = 8), AhR KO Ctrl (n = 4), AhR KO Alc (n = 4), and AhR KO Alc P (n = 5) mice. (**b**) Representative images of liver sections stained with hematoxylin-eosin, scale bar 100 µm. (**c,d**) Colon mRNA levels determined by qPCR: *cyp1a1*, *ahr*, *il22*, *reg3β* and *reg3γ*, normalized to that of the *18s* gene, in WT Ctrl (n = 8), WT Alc (n = 5), WT Alc P (n = 8), AhR KO Ctrl (n = 4), AhR KO Alc (n = 4), and AhR KO Alc P (n = 5) mice. Results are shown as the mean ± SEM. Significant results for *p < 0.05, **p < 0.01, and ***p < 0.001 were determined by Mann-Whitney tests unless stated otherwise.

Figure 5. Tryptophan metabolism is reduced in patients with severe alcoholic hepatitis (sAH) and correlates with disease severity. (**a**) Serum concentrations of tryptophan, kynurenine, and AHR agonists (tryptamine, indole, indole 3-acetic acid, indole 3-acetaldehyde, and indoxyl sulfate) in sAH patients (n = 14) and patients without severe alcoholic hepatitis (noAH, n = 15). (**b**) Spearman correlation of the serum tryptophan and AST, bilirubin, and prothrombin time levels and MELD score.

Figure 1

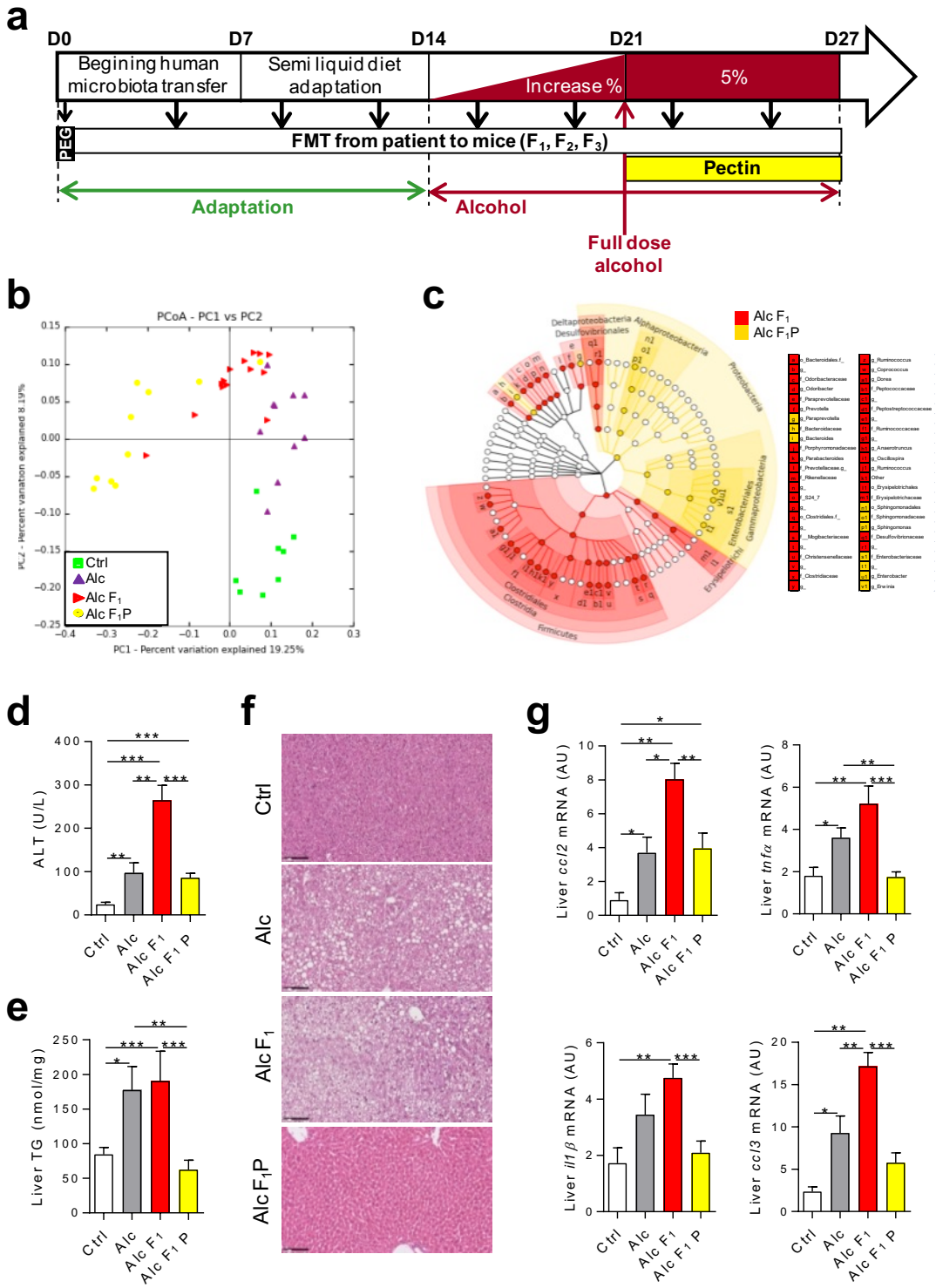
a
D0
D7
D14
D21
D27
Begining human microbiota transfer
Semi liquid diet adaptation
Increase %
5%
PEG
FMT from patient to mice (F1, F2, F3)
Pectin
Adaptation
Alcohol
Full dose alcohol
b
PCoA - PC1 vs PC2
PC1 - Percent variation explained 19.25%
PC2 - Percent variation explained 9.19%
Ctrl
Alc
Alc F1
Alc F1P
c
Alc F1
Alc F1P
Deltaproteobacteria
Desulfovibrionales
Alphaproteobacteria
Proteobacteria
Enterobacteriales
Gammaproteobacteria
Erysipelotrichi
Clostridiales
Clostridia
Firmicutes
d
ALT (U/L)
e
Liver TG (nmol/mg)
f
Ctrl
Alc
Alc F1
Alc F1P
g
Liver ccl2 mRNA (AU)
Liver tnfα mRNA (AU)
Liver il1β mRNA (AU)
Liver ccl3 mRNA (AU)
Ctrl
Alc
Alc F1
Alc F1 P

Figure 2

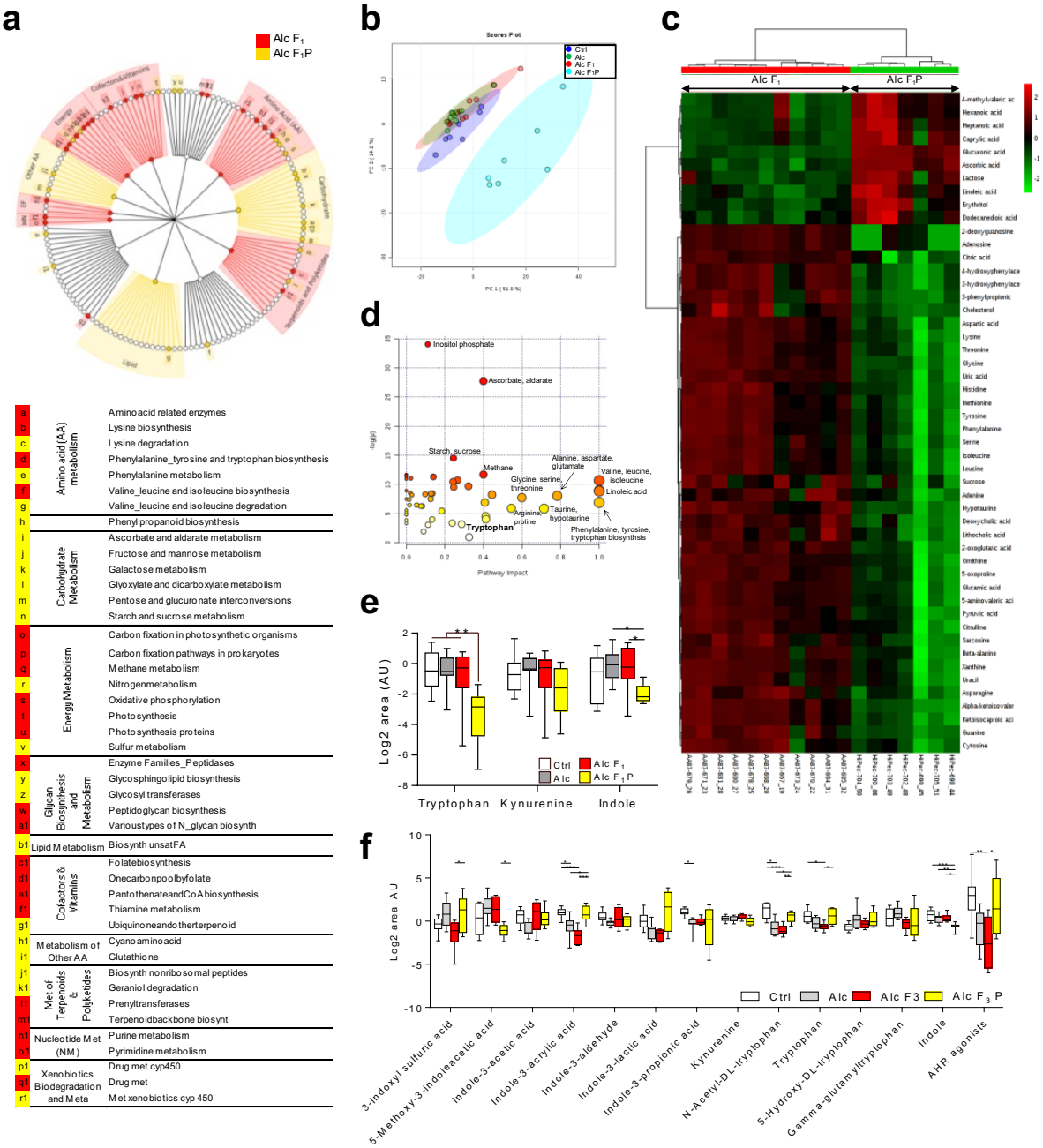

a	Amino acid (AA) metabolism	Aminoacid related enzymes
b		Lysine biosynthesis
c		Lysine degradation
d		Phenylalanine_tyrosine and tryptophan biosynthesis
e		Phenylalanine metabolism
f		Valine_leucine and isoleucine biosynthesis
g		Valine_leucine and isoleucine degradation
h		Phenyl propanoid biosynthesis
i	Carbohydrate Metabolism	Ascorbate and aldarate metabolism
j		Fructose and mannose metabolism
k		Galactose metabolism
l		Glyoxylate and dicarboxylate metabolism
m		Pentose and glucuronate interconversions
n		Starch and sucrose metabolism
o	Energy Metabolism	Carbon fixation in photosynthetic organisms
p		Carbon fixation pathways in prokaryotes
q		Methane metabolism
r		Nitrogenmetabolism
s		Oxidative phosphorylation
t		Photosynthesis
u		Photosynthesis proteins
v		Sulfur metabolism
x	Glycan Biosynthesis and Metabolism	Enzyme Families_Peptidases
y		Glycosphingolipid biosynthesis
z		Glycosyl transferases
w		Peptidoglycan biosynthesis
a1		Varioustypes of N_glycan biosynth
b1	Lipid Metabolism	Biosynth unsatFA
c1	Cofactors & Vitamins	Folatebiosynthesis
d1		Onecarbonpoolbyfolate
e1		PantothenateandCoAbiosynthesis
f1		Thiamine metabolism
g1		Ubiquinoneandotherterpenoid
h1	Metabolism of Other AA	Cyanoaminoacid
i1		Glutathione
j1	Met of Terpenoids & Polyketides	Biosynth nonribosomal peptides
k1		Geraniol degradation
l1		Prenyltransferases
m1		Terpenoidbackbone biosynt
n1	Nucleotide Met (NM)	Purine metabolism
o1		Pyrimidine metabolism
p1	Xenobiotics Biodegradation and Meta	Drug met cyp450
q1		Drug met
r1		Met xenobiotics cyp 450

1

2

Figure 3

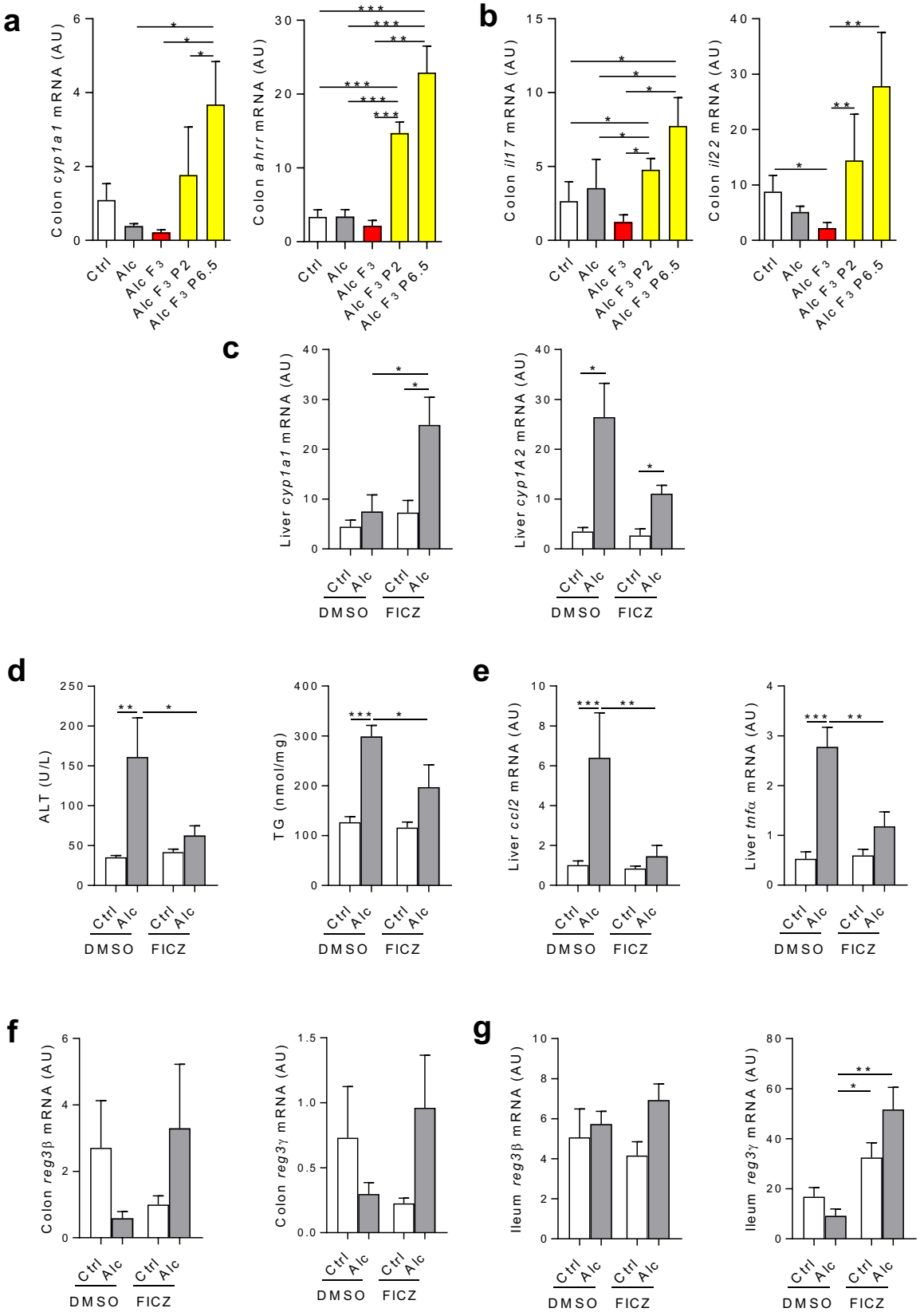
a
Colon cyp1a1 mRNA (AU)
Colon ahrr mRNA (AU)
b
Colon il17 mRNA (AU)
Colon il22 mRNA (AU)
Ctrl
Alc
Alc F3
Alc F3 P2
Alc F3 P6.5
c
Liver cyp1a1 mRNA (AU)
Liver cyp1A2 mRNA (AU)
DMSO
FICZ
d
ALT (U/L)
TG (nmol/mg)
e
Liver ccl2 mRNA (AU)
Liver tnfα mRNA (AU)
f
Colon reg3β mRNA (AU)
Colon reg3γ mRNA (AU)
g
Ileum reg3β mRNA (AU)
Ileum reg3γ mRNA (AU)

Figure 4

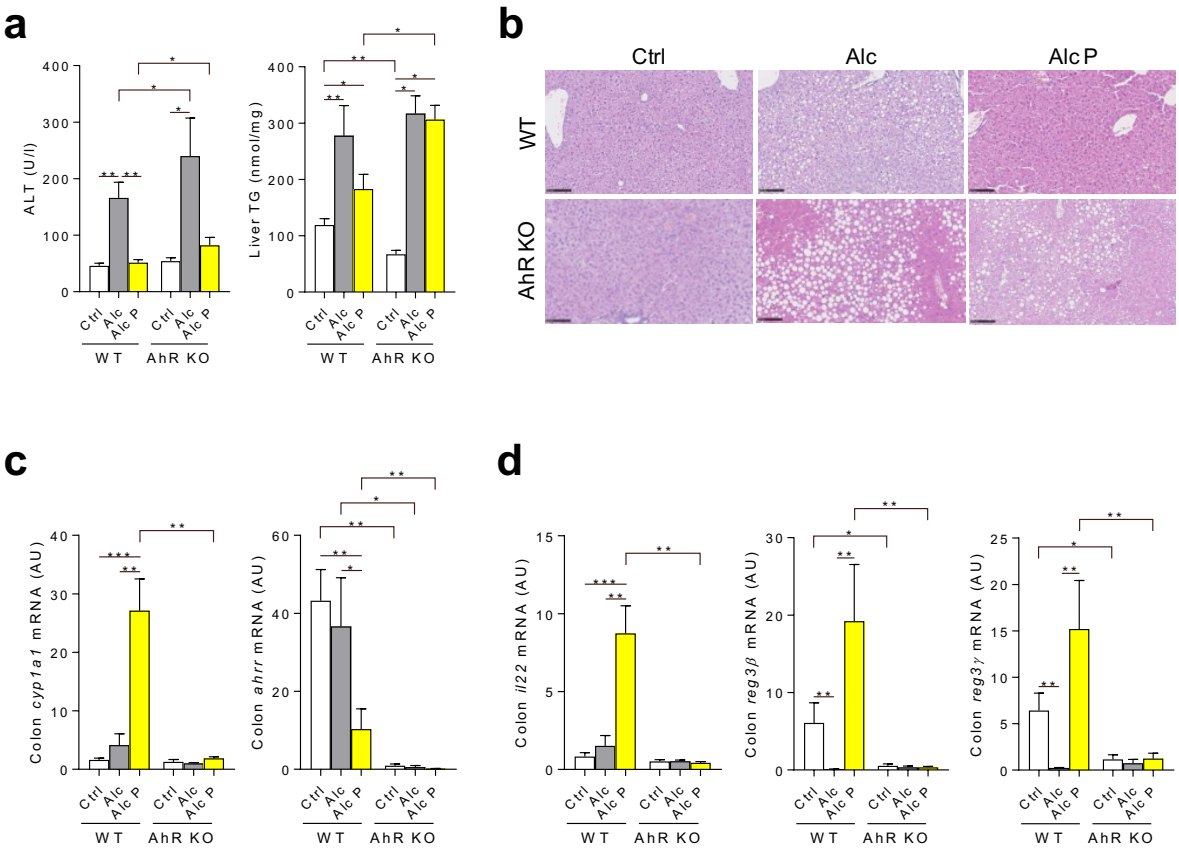
a
ALT (U/l)
Liver TG (nmol/mg)
Ctrl
Alc
Alc P
WT
AhR KO
b
Ctrl
Alc
Alc P
WT
AhR KO
c
Colon cyp1a1 mRNA (AU)
Colon ahrr mRNA (AU)
d
Colon il22 mRNA (AU)
Colon reg3β mRNA (AU)
Colon reg3γ mRNA (AU)

1

2

Figure 5

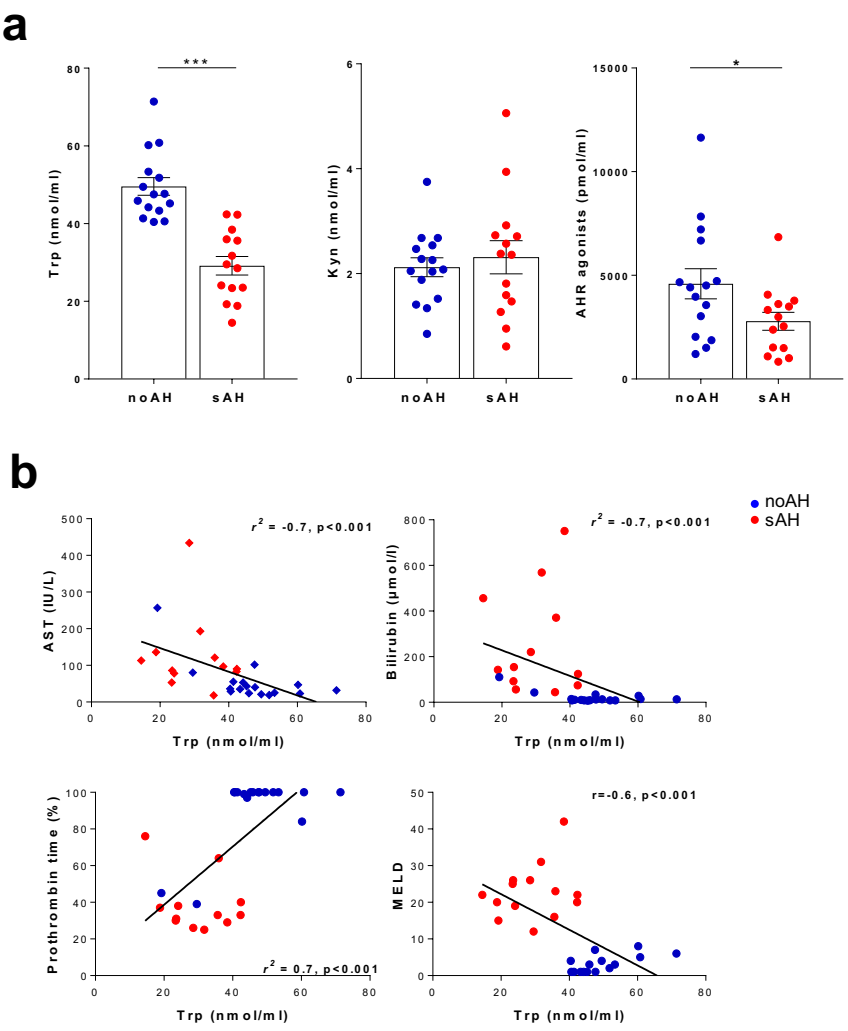
a
***
*
Trp (nmol/ml)
Kyn (nmol/ml)
AHR agonists (pmol/ml)
noAH
sAH
b
noAH
sAH
AST (IU/L)
Bilirubin (µmol/l)
Prothrombin time (%)
MELD
Trp (nmol/ml)
r² = -0.7, p<0.001
r² = 0.7, p<0.001
r=-0.6, p<0.001

1

2

SUPPLEMENTARY DATA

Material and methods	**4**
Supplementary Figure 1	**10**
Supplementary Figure 2	**11**
Supplementary Figure 3	**12**
Supplementary Figure 4	**13**
Supplementary Figure 5	**14**
Supplementary Figure 6	**15**
Supplementary Figure 7	**16**
Supplementary Figure 8	**17**
Supplementary Table 1	**18**
Supplementary Table 2	**19**
Supplementary Table 3	**22**
Supplementary Table 4	**24**
Supplementary Table 5	**25**

MATERIAL AND METHODS

Chronic exposure to alcohol. Eight-week old mice were fed a liquid diet adapted from Lieber DeCarli for 21 days, as previously described based on the NIAAA model [3] but without a binge administration of alcohol at the end. Briefly, the ethanol diet was obtained by adding absolute ethanol to a solution of Lieber DeCarli powder (Ssniff, Spezialdiäten GmbH, Soest, Germany) in filtered water. After a 7-day period of adaptation to the animal facility and a 7-day period adaptation to the semi-liquid diet, mice were given increasing amounts of ethanol for 7 days (1% increase every two days). The final concentration of ethanol in this liquid diet was 5% (vol/vol), such that ethanol accounted for 28% of the total caloric intake. The control diet was obtained by replacing the ethanol with an isocaloric amount of maltodextrin (Maldex 170, Safe, France). Alcohol-fed groups were allowed free access to the 5% (vol/vol) ethanol diet for 7 days. Control mice were fed the isocaloric control diet throughout the entire feeding period. During the Lieber DeCarli diet, animals did not have access to drinking water. Diet consumptions were recorded and were similar between the groups (data not shown).

Tissues and samples. Mice were anesthetized and blood samples collected in EDTA coated tubes. Liver and distal colon were excised: one piece was fixed in buffered formaldehyde and another piece was snap-frozen in liquid nitrogen for TG and RNA extractions. All samples were stored at -80°C until use. Fecal samples were collected from mice immediately before euthanasia.

Measurement of bacterial translocation in the liver. Liver were collected in sterile conditions and disrupted in 2 ml of PBS 1X. 500 µl of lysate were put on PolyVitex chocolate agar (Biomérieux, Capronne, France), spread with balk and place in incubator in anaerobic conditions at 37°C during 48 to 72 hours and colony-forming unit were counted.

Measurement of liver triglycerides and blood samples. Liver triglycerides were extracted using a triglyceride quantification kit following the manufacturer's indications (Abcam, Cambridge, UK). Quantification was performed by using a Berthold Technologies colorimetric microplate reader (Mithras LB 940), and the level of liver TG was expressed in nmol per milligram of liver. Plasma alanine aminotransferase (ALT), aspartate transaminase (AST), triglycerides, high-density lipoprotein (HDL) and cholesterol levels were assed using a spectrophotometric method

(Olympus, AU400). Alcohol was measured in the plasma by using the colorimetric assay kit (Biovision).

Liver and gut histology. Liver and gut (colon) were fixed overnight in 4% paraformaldehyde and embedded in paraffin. Paraffin sections (4 µm thick) were stained with hematoxylin and eosin (H&E). Colon samples were also stained with Alcian Blue.

Immunofluorescence. Specimens were embedded in paraffin and cut in 3-µm section. Staining with antibodies purchased from abcam against ZO-1 (ab96587) and occludine (ab216327) was done, followed by staining with a fluorochrome-coupled secondary antibody goat anti-rabbit Alexa FluorTM Plus 594 (Invitrogen, Thermo Fisher Scientific). Nuclei were stained with Hoechst (Life Technologies, Thermo Fisher Scientific). Slides were scanned by the digital slide scanner NanoZoomer 2.0-RS (Hamamatsu, France) allowing an overall view of the samples. Images were digitally captured from the scanned slides using the NDP.view2 software (Hamamatsu, France).

RNA extraction and quantification. Mice livers were disrupted in Qiazol solution. Total RNA was extracted using a Qiagen RNeasy Lipid tissue minikit (Courtaboeuf, France). Total gut RNA was extracted using a Qiagen RNeasy Plus Mini Kit (Courtaboeuf, France), after being disrupted with an MP Biomedicals FastPrep. The RNA integrity number (RIN) was determined using an Agilent Bioanalyzer 2100 system with the RNA 6000 Nano Labchip kit. Samples with a RIN of less than 8 were eliminated. For cDNA synthesis, 1 µg of each total RNA sample was reverse transcribed. A 12 µl mix containing 1 µg of RNA, random hexamers (Roche Diagnostics, Meylan, France), and 10 mM dNTP Mix (Invitrogen, Carslbad, CA) was prepared for each sample. Mixtures were heated at 65°C for 5 min, cooled on ice, and then an 8 µl reaction mix containing 1 µl M-MuLv RT (Invitrogen), 4 µl 5x Buffer (Invitrogen), 2 µl 0.1 M dithiothreitol (Invitrogen), and 1 µl Protector RNase Inhibitor (40 U/µl; Invitrogen) was added. The reaction conditions were 10 min at 25°C, 50 min at 50°C, 15 min at 70°C.

Gene expression analysis by quantitative qPCR. Real-time qPCR was performed in a Light Cycler 480 (Roche Diagnostics) using the LC FastStart DNA Master SYBR Green I kit (Roche Diagnostics). Amplification was initiated with an enzyme activation step at 95°C for 10 min, followed by 40 cycles consisting of a 20 s denaturation step at 95°C, a 15 s annealing step at the temperature appropriate for each primer, and a 45 s elongation step at 72°C. We amplified

the cDNAs for *18s*, *gapdh*, *tnfα*, *tgfβ*, *il1β*, *ccl2*, *ccl3*, *reg3b*, *reg3g*, *il22*, *il17*, *ahrr* and *cyp1a1*. Primer sequences are listed in Supplemental Table 5. Data were analyzed using Light Cycler 480 Software (Roche Diagnostics). Relative gene expression was normalized to the *18s* or *gapdh* reference gene.

Analysis of the intestinal microbiota by 16S RNA sequencing. The composition of the microbiota was analyzed using Illumina MiSeq technology targeting the 16S ribosomal DNA V3-V4 region in paired-end modus (2 x 300 base pair) (GenoToul, Toulouse). Bacterial DNA was obtained by homogenizing stools in a Guanidinium thiocyanate containing lysis buffer using a Fast Prep homogenizer. High quality bacterial DNA was extracted by successive steps of purification and precipitation using "Laboratory-made" buffers [4]. PCR were performed to prepare amplicons using V3-V4 oligonucleotides (PCR1F_460: 5' CTTTCCCTACACGACGCTCTTCCGATCTACGGRAGGCAGCAG 3', PCR1R_460: 5' GGAGTTCAGACGTGTGCTCTTCCGATCTTACCAGGGTATCTAATCCT 3'). Amplicon quality was verified by gel electrophoresis and they were sent to the GenoToul plateform for sequencing. The resulting paired reads were assembled using PANDAseq v 2.7 to generate an amplicon size of 450 base pairs [5]. Reads were demultiplexed and processed using the quantitative insights into microbial ecology (QIIME v1.9.0) pipeline and the default parameters of QIIME[6]. Chimeric sequences were identified *de novo*, reference based, and then removed using usearch61 [7]. The non-chimeric sequences were then clustered into operational taxonomic units (OTUs) at 97.0% sequence similarity using a closed reference-based picking approach with UCLUST software against the Greengenes database 13_8 of bacterial 16S rDNA sequences [8]. The mean number of quality-controlled reads was 25034 ± 6875 (mean ± SD) per sample. After rarefaction at 7,000 reads per sample, bacterial alpha diversity was estimated using Shannon index. OTUs with a prevalence < 5% were removed from the analysis. Analyses using R software v2.14.1 were restricted to merged OTUs with the same taxonomic assignment. Results are represented as the mean ± SEM. The Wilcoxon test was used to assess statistical significance of the bacterial composition between the different samples. Associations were considered to be significant after a false-discovery rate (FDR) correction of the p-value ($q < 0.05$).

Beta diversity was assessed using weighted and unweighted UniFrac distances. The weighted Unifrac metric is weighted by the difference in the abundance of OTUs from each community, whereas unweighted Unifrac only considers the absence/presence of the OTUs providing different information. The link between the different groups of mice and bacterial microbial

profiles was addressed by performing an ANOSIM test with 10,000 permutations on the beta diversity metrics described above.

Functional composition of the intestinal metagenome was predicted using Phylogenetic Investigation of Communities by Reconstruction of Unobserved States (PICRUSt) [9]. This is a computational approach that accurately predicts the abundance of gene families in the microbiota and thus provides information about the functional composition of the microbial community. Linear discriminant analysis (LDA) effect size (LEfSe) analysis was performed to identify the taxa and functions displaying the largest differences in abundance in the microbiota between groups [10]. Only taxa and functions with an LDA score > 2 and a significance of < 0.05, as determined by Wilcoxon signed-rank tests, are shown. LEfSe and PICRUSt were accessed online (http://huttenhower.sph.harvard.edu/galaxy/).

Analysis of fecal metabolites by gas chromatography coupled to a triple quadrupole mass spectrometer. Fecal metabolites were measured using the GC-MS/MS method as previously described [11]. Briefly, about 20 mg of biological material for each sample were first weighted and solubilized into microcentrifuge tubes with 500 µL of MilliQ water (+4°C). Samples were snap frozen in liquid nitrogen, then thaw at room temperature on the bench, while they were thoroughly vortex. Samples were splitted in two parts: the first 200 µl were added to 300 µl of cold methanol, the others 200 µl were added to 300 µl of cold TBME. The two aliquots were centrifugated 10 minutes at 15000g (+4 °C). Concerning the TBME extraction, the upper layer was transferred in vial for direct injection into Gas Chromatography coupled with Mass Spectrometry (GC/MS, WAX method). Concerning the methanol extraction, 400 µl of the supernatant were transferred and evaporated in microcentrifuge tubes at 40°C in a pneumatically assisted concentrator (Techne DB3, Staffordshire, UK). On dried extract, 300 µl of methanol were added then splitted in two aliquots: the first 150 µL used for GC/MS (HP5MS method) experiment in vial injection, the others 150 µL used for the Ultra High Pressure Liquid Chromatography coupled by Mass Spectrometry (UHPLC/MS) experimentations. Concerning the GC/MS (HP5MS) aliquots, the 150 µL were evaporated and 50 µL of methoxyamine (20 mg/mL in pyridine) was added on dried extracts, and stored at room temperature in dark, during 16 hours. The day after, 80 µL of MSTFA was added and final derivatization occurred at 40°C during 30 minutes. Samples were then directly injected into GC-MS.

Concerning the LC-MS aliquots, the collected supernatant was evaporated in microcentrifuge tubes at 40°C in a pneumatically assisted concentrator (Techne DB3, Staffordshire, UK). The LC-MS dried extracts were solubilized with 450 µL of MilliQ water and aliquoted in 3

microcentrifuge tubes (100 µL) for each LC method and one microcentrifuge tube for backup. Aliquots for analysis were transferred in LC vials and injected into UHPLC/MS or kept at -80°C until injection.

The GC-MS/MS method was performed on a 7890B gas chromatography (Agilent Technologies, Waldbronn, Germany) coupled to a triple quadrupole 7000C (Agilent Technologies, Waldbronn, Germany) equipped with a High sensitivity electronic impact source (EI) operating in positive mode.

The front inlet temperature was 250°C, the injection was performed in splitless mode. The transfer line and the ion-source temperature were 250°C and 230°C, respectively. The septum purge flow was fixed at 3 mL/min, the purge flow to split vent operated at 80 mL/min during 1 min and gas saver mode was set to 15 mL/min after 5 min.

The helium gas flowed through the column (J&WScientificHP-5MS, 30m x 0.25 mm, i.d. 0.25 mm, d.f., Agilent Technologies Inc.) at 1 mL/min. Column temperature was held at 60°C for 1 min, then raised to 210°C (10°C/min), followed by a step to 230°C (5°C/min) and reached 325°C (15°C/min), and be hold at this temperature for 5 min.

The scan mode used was the MRM for biological samples. Peak detection and integration of the analytes were performed using the Agilent Mass Hunter quantitative software (B.07.01).

All the statistical analysis and pathway annotations for the metabolites were carried out using MetaboAnalyst web tool (www.metaboanalyst.ca) [12]. Data was normalized using log transformation and Pareto-scaling. For multi group analysis, one-way ANOVA was performed followed by post-hoc analyses using Tukey's HSD. For predicting variance in samples, Principal Component Analysis (PCA) was performed. The significant pathways involved in the pectin effect were also identified using MetaboAnalyst tool [13].

Measurement of tryptophan metabolites in the feces and plasma of patients. Indole derivatives were quantified HPLC-coupled to high resolution mass spectrometry as previously described [14].

REFERENCES

1-Llopis M*, et al.* (2016) *Gut* 65(5):830-839.
2-Wrzosek L*, et al.* (2018) *Sci Rep* 8(1):6854.
3-Bertola A*, et al.* (2013) *Nature protocols* 8(3):627-637.
4-Tomas J*, et al.* (2013) *FASEB J.* 27(2):645-655.
5-Masella AP*, et al.* (2012) *BMC Bioinformatics* 13:31.

6-Caporaso JG*, et al.* (2010) *Nat Methods* 7(5):335-336.
7-Edgar RC (2010) *Bioinformatics* 26(19):2460-2461.
8-DeSantis TZ*, et al.* (2006) *Appl. Environ. Microbiol.* 72(7):5069-5072.
9-Langille MG*, et al.* (2013) *Nat. Biotechnol.* 31(9):814-821.
10-Segata N*, et al.* (2011) *Genome Biol* 12(6):R60.
11-Pietrocola F*, et al.* (2017) *Autophagy* 13(12):2163-2170.
12-Chong J*, et al.* (2018) *Nucleic Acids Res* 46(W1):W486-W494.
13-Xia J*, et al.* (2016) *Curr Protoc Bioinformatics* 55:14 10 11-14 10 91.
14-Lefevre A*, et al.* (2019) *Talanta* 195:593-598.

Supplementary Figure 1

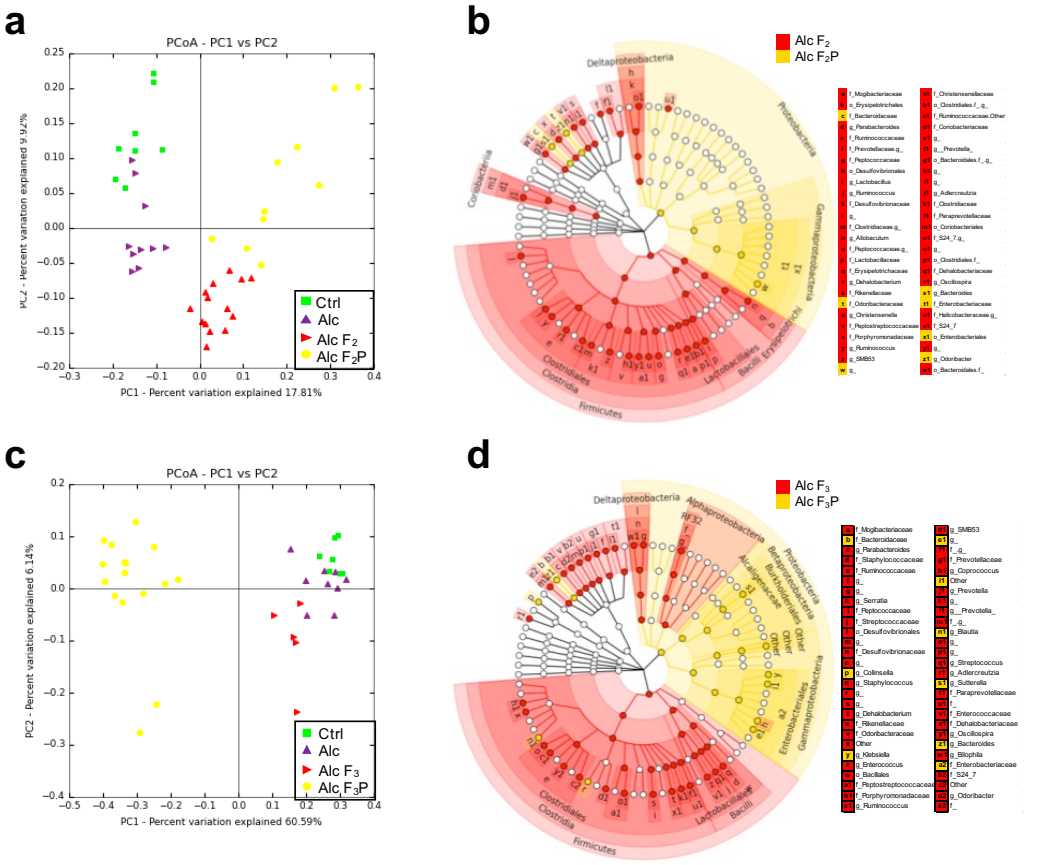

Supplementary Figure 1. The composition of the intestinal microbiota of mice humanized with feces from two patients with severe alcoholic hepatitis is modified by pectin treatment. Ctrl, control-fed mice; Alc, alcohol-fed mice; Alc F2 and Alc F3, alcohol-fed mice humanized with the microbiota from a patient with sAH (patient F2 or F3); Alc F2 P6.5 and Alc F3 P6.5, alcohol-fed mice humanized with the microbiota from a patient with sAH (patient F2 or F3) and treated with 6.5% pectin. (**a**) Principal Coordinate Analysis (PCoA) plot showing the unweighted UniFrac distance ($p < 0.001$, R= 0.59, ANOSIM test, 10,000 permutations, using the first 5 PC). (**b**) Cladograms showing the taxa most differentially associated with Alc F2 (red) or Alc F2 P6.5 mice (yellow) (Wilcoxon rank-sum test). Circle sizes in the cladogram plot are proportional to bacterial abundance. The circles represent, going from the inner to outer circle: phyla, genus, class, order, and family. Mice per group for **a** and **b**: Ctrl (n=8), Alc (n=10), Alc F2 (n=15), and Alc F2 P6.5 (n=10). (**c**) PCoA plot showing the unweighted UniFrac distance ($p < 0.001$, R= 0.68, ANOSIM test, 10,000 permutations, using the first 5 PC). (**d**) Cladograms showing the taxa most differentially associated with Alc F3 (red) or Alc F3 P6.5 mice (yellow) (Wilcoxon rank-sum test). Mice per group in **c** and **d**: Ctrl (n=7), Alc (n=9), Alc F3 (n=5), Alc F3 P0.4 (n=8), Alc F3 P1 (n=11), Alc F3 P2 (n= 16), and Alc F3 P6.5 (n=16).

Supplementary Figure 2

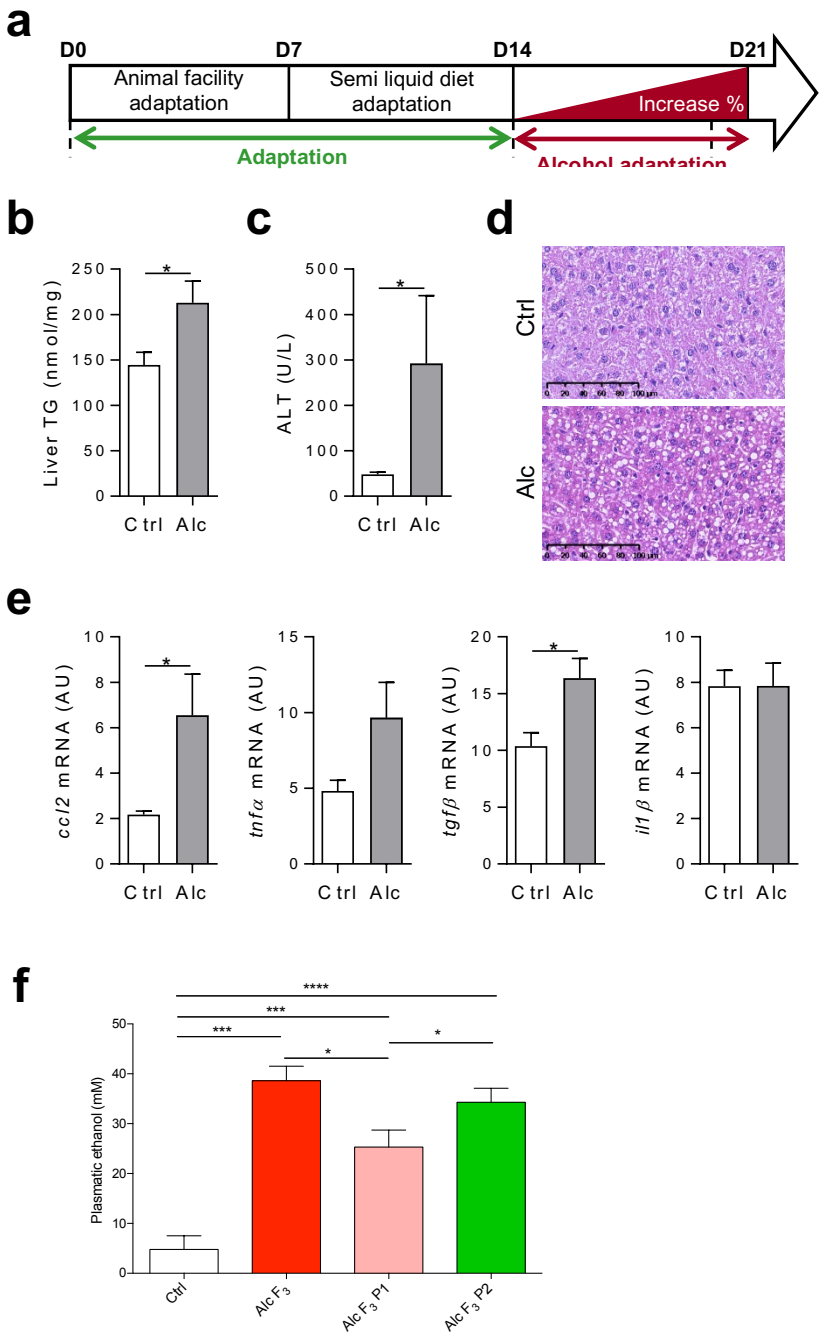

Supplementary Figure 2. Alcohol-induced liver injury after the alcohol adaptation period. Ctrl, control-fed mice (n=11); Alc, alcohol-fed mice (n=11). (**a**) Experimental design: mice were progressively adapted to a semi-liquid, Lieber DeCarli (LDC) diet, then to an ethanol diet, using increasing doses of ethanol (2-4%) for seven days. (**b**) ALT level. (**c**) Liver triglyceride quantification. (**d**) Representative pictures of liver sections stained with haematoxylin-eosin in control and alcohol-fed mice showing steatosis, scale bar 100 µm. (**e**) Liver mRNA levels of inflammation markers were determined by qPCR: *ccl2, tnfα, tgfβ*, and *il1β*, normalized to that of the *gapdh* gene. (**f**) Plasmatic alcohol in control mice (Ctrl) and alcohol fed mice transplanted with MI of sAH patient (Alc sAH) and treated with 1% or 2% of pectin. Results are shown as the mean ± SEM. Significant results for *p < 0.05, ***p < 0.0002, ****p < 0.0001 were determined by the Mann-Whitney test.

Supplementary Figure 3

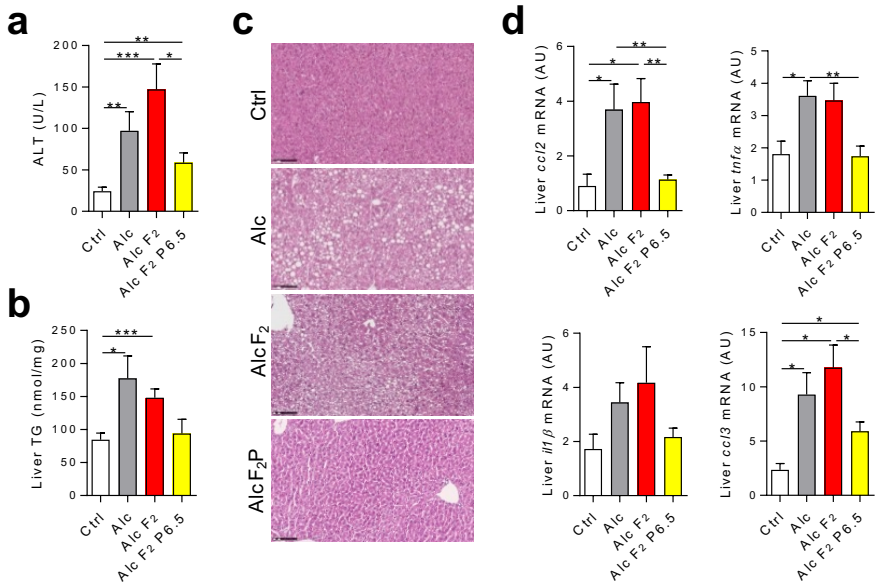

Supplementary Figure 3. Pectin treatment reverses liver lesions in mice humanized with the intestinal microbiota from a patient with severe alcoholic hepatitis. Ctrl, control-fed mice; Alc, alcohol-fed mice; Alc F2, alcohol-fed mice humanized with the microbiota from a patient with sAH (patient F2); Alc F2 P6.5, alcohol-fed mice humanized with the microbiota from a patient with sAH (patient F2) and treated with 6.5% pectin. (**a**) ALT level in Ctrl (n=8), Alc (n=8), Alc F2 (n=16), and Alc F2 P6.5 (n=10) mice. (**b**) Liver triglyceride quantification in Ctrl (n=8), Alc (n=8), Alc F2 (n=14), and Alc F2 P6.5 (n=8) mice. (**c**) Representative images of liver sections stained with haematoxylin-eosin, scale bar 100 µm. (**d**) Liver mRNA levels determined by qPCR: *ccl2, tnfα, il1β* and *ccl3* normalized to that of the *gapdh* gene in Ctrl (n=4), Alc (n=5), Alc F2 (n=16), and Alc F2 P6.5 (n=9) mice. Results are shown as the mean ± SEM. Significant results for *p < 0.05, **p < 0.01, and ***p < 0.001 were determined by Mann-Whitney tests unless stated otherwise.

Supplementary Figure 4

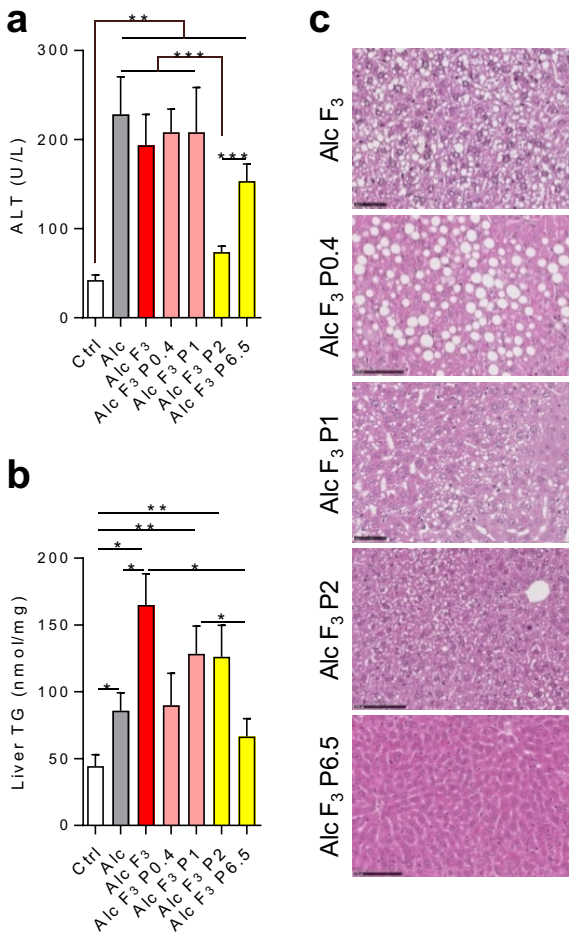

Supplementary Figure 4. Dose-dependent effect of pectin on liver and intestinal barrier function. Ctrl, control-fed mice; Alc, alcohol-fed mice; Alc F3, alcohol-fed mice humanized with the microbiota from a patient with sAH (patient F3); Alc F3 P0.4, Alc F3 P1, Alc F3 P2, and Alc F3 P6.5, alcohol-fed mice humanized with the microbiota from a patient with sAH (patient F3) and treated with 0.4, 1, 2, or 6.5% pectin, respectively. (a) ALT levels in Ctrl (n=8), Alc (n=9), Alc F3 (n=6), Alc F3 P0.4 (n=9), Alc F3 P1 (n=12), Alc F3 P2 (n=15), and Alc F3 P6.5 (n=16) mice. (b) Liver triglyceride quantification in Ctrl (n=8), Alc (n=9), Alc F3 (n=3), Alc F3 P0.4 (n=7), Alc F3 P1 (n=10), Alc F3 P2 (n=16), and Alc F3 P6.5 (n=14) mice. (c) Representative images of liver sections stained with haematoxylin-eosin, scale bar 400 µm. Results are shown as the mean ± SEM. Significant results for *p < 0.05, **p < 0.01, and ***p < 0.001 were determined by Mann-Whitney tests unless stated otherwise.

Supplementary Figure 5

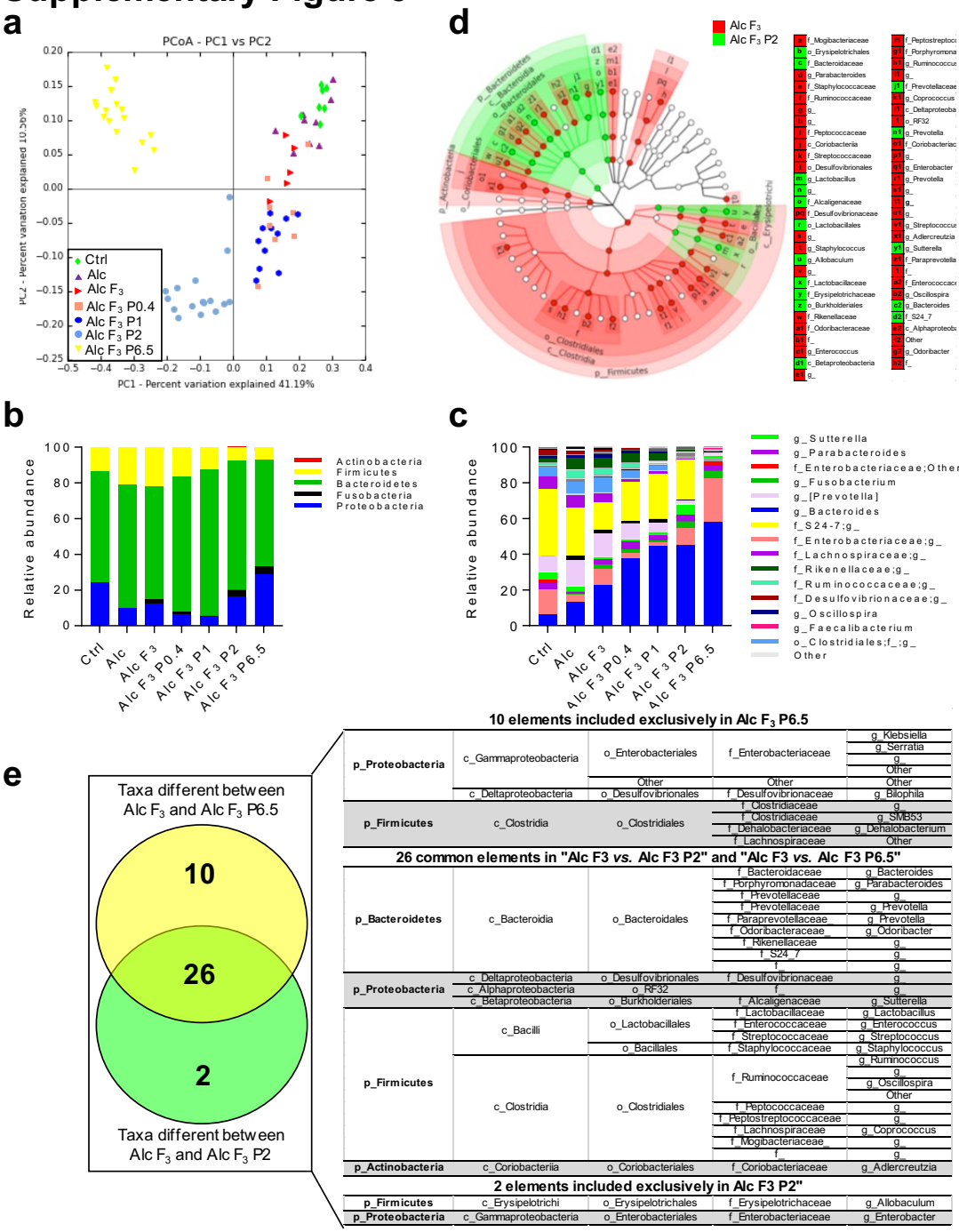

10 elements included exclusively in Alc F_3 P6.5

p_Proteobacteria	c_Gammaproteobacteria	o_Enterobacteriales	f_Enterobacteriaceae	g_Klebsiella
				g_Serratia
				g_
			Other	Other
	c_Deltaproteobacteria	o_Desulfovibrionales	f_Desulfovibrionaceae	g_Bilophila
p_Firmicutes	c_Clostridia	o_Clostridiales	f_Clostridiaceae	g_
			f_Clostridiaceae	g_SMB53
			f_Dehalobacteriaceae	g_Dehalobacterium
			f_Lachnospiraceae	Other

26 common elements in "Alc F3 *vs.* Alc F3 P2" and "Alc F3 *vs.* Alc F3 P6.5"

p_Bacteroidetes	c_Bacteroidia	o_Bacteroidales	f_Bacteroidaceae	g_Bacteroides
			f_Porphyromonadaceae	g_Parabacteroides
			f_Prevotellaceae	g_
			f_Prevotellaceae	g_Prevotella
			f_Paraprevotellaceae	g_Prevotella
			f_Odoribacteraceae	g_Odoribacter
			f_Rikenellaceae	g_
			f_S24-7	g_
			f_	g_
p_Proteobacteria	c_Deltaproteobacteria	o_Desulfovibrionales	f_Desulfovibrionaceae	g_
	c_Alphaproteobacteria	o_RF32	f_	g_
	c_Betaproteobacteria	o_Burkholderiales	f_Alcaligenaceae	g_Sutterella
p_Firmicutes	c_Bacilli	o_Lactobacillales	f_Lactobacillaceae	g_Lactobacillus
			f_Enterococcaceae	g_Enterococcus
			f_Streptococcaceae	g_Streptococcus
		o_Bacillales	f_Staphylococcaceae	g_Staphylococcus
	c_Clostridia	o_Clostridiales	f_Ruminococcaceae	g_Ruminococcus
				g_
				g_Oscillospira
				Other
			f_Peptococcaceae	g_
			f_Peptostreptococcaceae	g_
			f_Lachnospiraceae	g_Coprococcus
			f_Mogibacteriaceae	g_
			f_	g_
p_Actinobacteria	c_Coriobacteriia	o_Coriobacteriales	f_Coriobacteriaceae	g_Adlercreutzia

2 elements included exclusively in Alc F3 P2"

p_Firmicutes	c_Erysipelotrichi	o_Erysipelotrichales	f_Erysipelotrichaceae	g_Allobaculum
p_Proteobacteria	c_Gammaproteobacteria	o_Enterobacteriales	f_Enterobacteriaceae	g_Enterobacter

Supplementary Figure 5. Gut microbiota composition of mice humanized with intestinal microbiota from a patient with severe alcoholic and treated with different doses of pectin. Alc, alcohol-fed mice (n=5); Ctrl, control-fed mice (n=7); Alc F_3(n=5), alcohol-fed mice humanized with the microbiota from a patient with sAH (patient F_3) ; Alc F_3 P0.4 (n=8), Alc F_3 P1 (n=11), Alc F_3 P2 (n=16), Alc F_3 P6.5 (n=16), alcohol-fed mice humanized with the microbiota from a patient with sAH (patient F_3) and treated with pectin 0.4%, 1%, 2% or 6.5% respectively. (**a**) PCoA plot showing the unweighted UniFrac distance ($p < 0.001$, R= 0.75, ANOSIM test, 10,000 permutations, using the first 5 PC). (**b**) Bacterial taxon-based analysis at the phylum and (**c**) genus level in faecal microbiota (**d**) LDA effect size (LEfSe) cladograms showing the taxa most differentially associated with Alc F_3 (red) or Alc F_3 P2 mice (green) (Wilcoxon rank-sum test). Circle sizes in the cladogram plot are proportional to bacterial abundance. The circles represent, going from the inner circle to the outer circle: phyla, genus, class, order, and family. (**e**) Venn diagram based on the taxa different in LEfSe analysis between Alc F_3 vs. Alc F_3 P6.5 and Alc F_3 vs. Alc F_3 P2 and the corresponding common taxa between these two comparisons.

1

Supplementary Figure 6

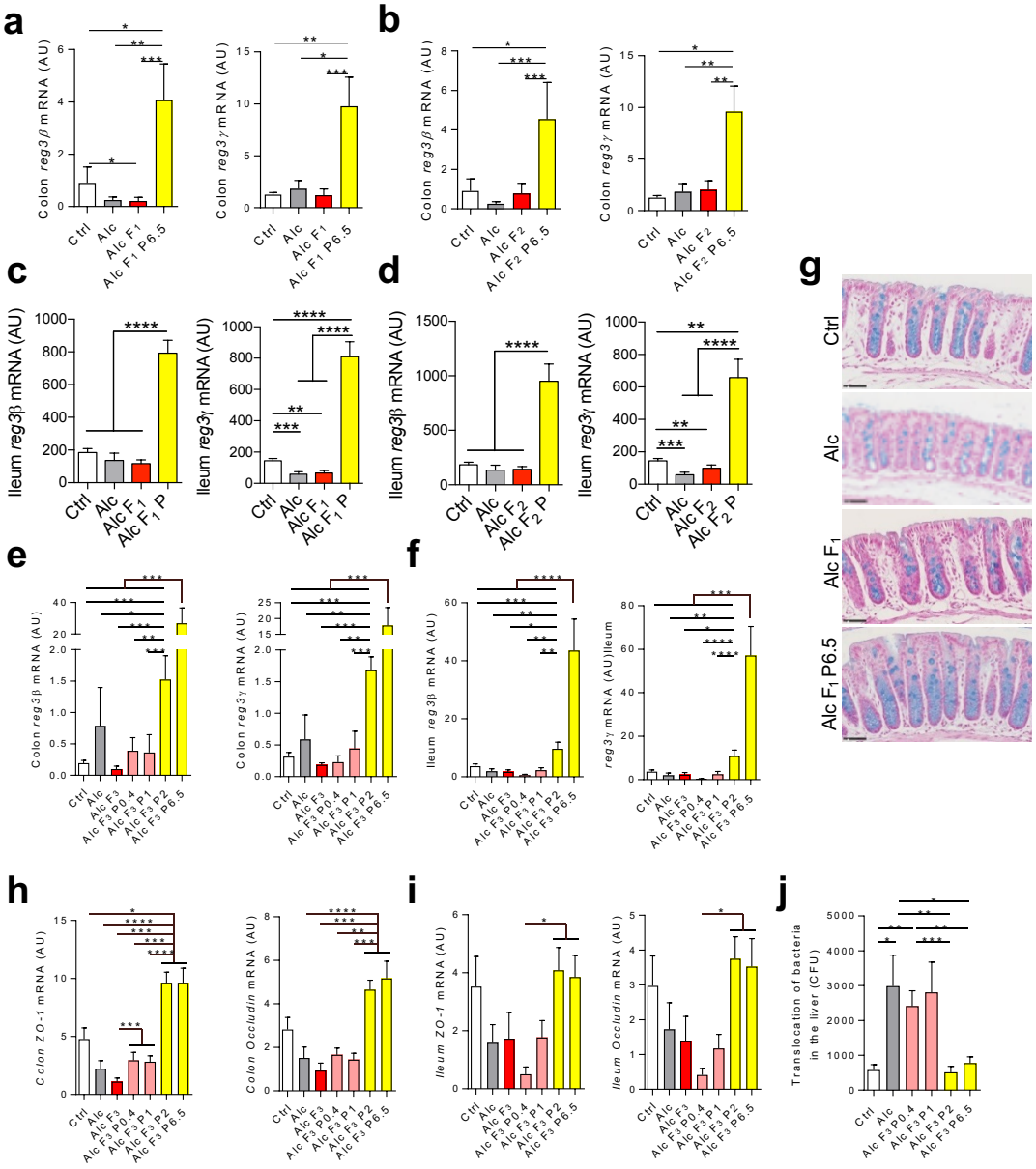

Supplementary Figure 6. Pectin treatment improves intestinal barrier function. Ctrl, control-fed mice; Alc, alcohol-fed mice; Alc F1, Alc F2 and Alc F3, alcohol-fed mice humanized with the microbiota from a patient with sAH (patients F1, F2 or F3); Alc F1 P6.5, Alc F2 P6.5 and Alc F3 P6.5, alcohol-fed mice humanized with the microbiota from a patient with sAH (patient 1, 2, or 3) and treated with 6.5% pectin. (a-f) Colon and ileum mRNA levels determined by qPCR: *reg3β* and *reg3γ* normalized to that of the *gapdh* gene. (e) Representative images of colon sections stained with Alcian blue, scale bar 50 µm. (h) Colon and (i) ileum mRNA levels determined by qPCR: *ZO-1* and *occludin* normalized to that of the *18s*gene. (j) Culture of bacteria in the liver. For a-d and g: Ctrl (n=8), Alc (n=8), Alc F1 (n=12), Alc F1 P6.5 (n=10), Alc F2 (n=16) and Alc F2 P6.5 (n=10) mice. For e-j: Ctrl (n=8), Alc (n=9), Alc F3 P0.4 (n=9), Alc F3 P1 (n=12), Alc F3 P2 (n=13), and Alc F3 P6.5 (n=13) mice. Results are shown as the mean ± SEM. Significant results for *p < 0.05, **p < 0.01, and ***p < 0.001 were determined by Mann-Whitney tests unless stated otherwise.

Supplementary Figure 7

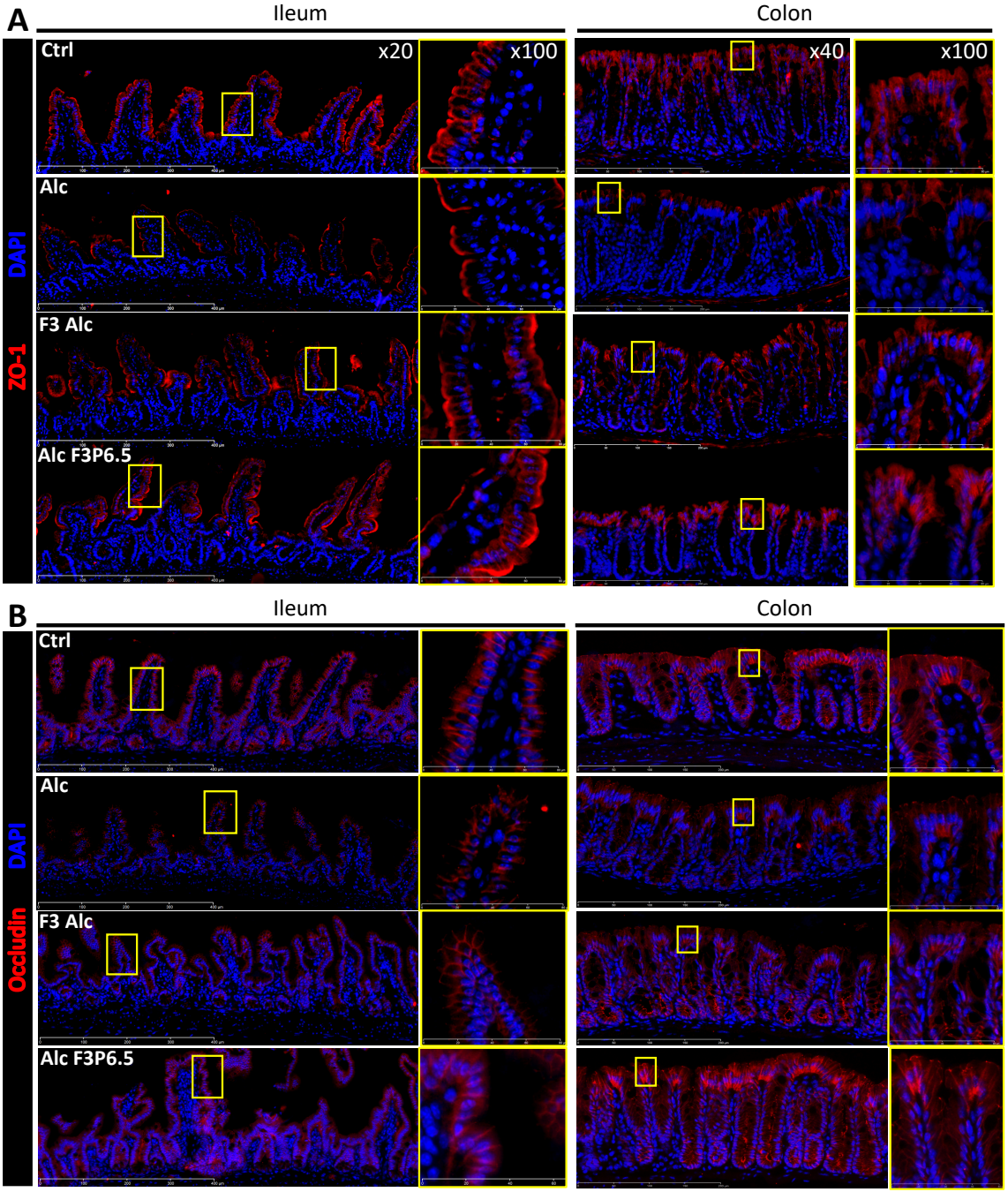

Supplementary Figure 7. Representative panels for the expression of tight junction proteins. (A) ZO-1 and (B) occludin expression in the ileum and colon.

Supplementary Figure 8

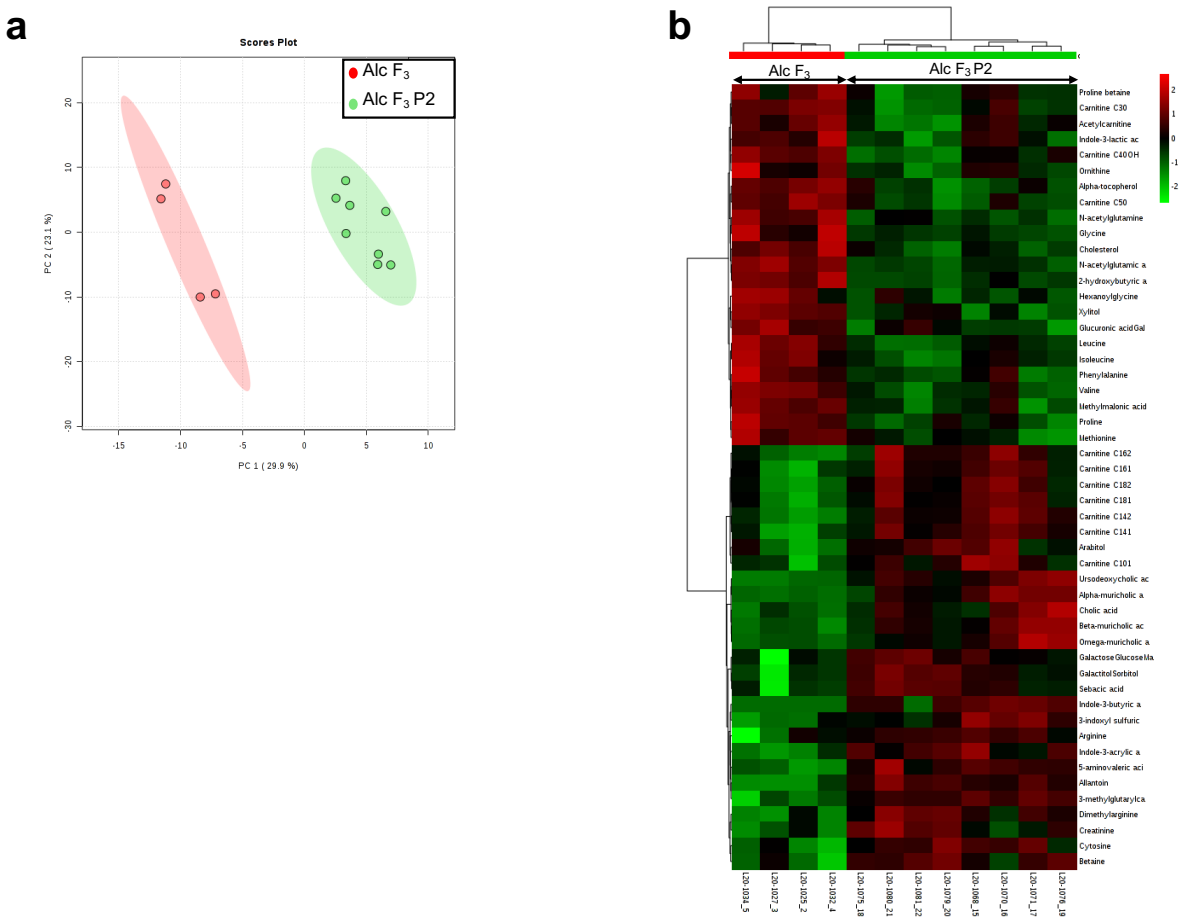

Supplementary Figure 8. The fecal metabolomic profile in mice humanized with intestinal microbiota from a patient with severe alcoholic hepatitis is modified by pectin. Alc F3 (n=4), alcohol-fed mice humanized with the microbiota from a patient with sAH (patient F3), Alc F3 P2 (n=8), alcohol-fed mice humanized with the microbiota from a patient with sAH (patient F3) and treated with 2% pectin. (**a**) PCA ordination plot of all fecal metabolomic data. (**b**) Heatmap showing the first 60 metabolites ranked by t-tests between Alc F3 (red) and Alc F3 P2 (green).

Supplementary table 1: Clinical characteristics of donor patients with severe alcoholic hepatitis.

Patient	F_1	F_2	F_3
Age (yr)	35	52	41
Alcohol consumption (g/d)	120	160	90
Duration of alcohol intake (yr)	16	20	18
BMI (kg/m2)	29	21	23
AST (IU/L)	193	153	434
Albumin (g/L)	23	27	21
Blood glucose (mmol/L)		5	5.6
Triglycerides (g/L)		0.81	1.37
PT (%)	25	30	26
Bilirubin (μmol/L)	569	92	220
Maddrey discriminant function	101	64	80
MELD	34	25	26

BMI: body mass index; AST: aspartate aminotransferase; PT: prothrombin time as percentage of control

Supplementary table 2: Predicted metabolomic pathways changes in intestinal microbiota

Picrust predicted metabolic pathways	Pathway	Alc F1 vs Alc F1 P6.5			Alc F2 vs Alc F2 P6.5			Alc F3 vs Alc F3 P6.5		
		Increased in	LDA	p	Increased in	LDA	p	Increased in	LDA	p
Metabolism of Cofactors and Vitamins	One carbon pool by folate	AlcF1	2.55	0.00	AlcF2	2.48	0.00	AlcF3	2.78	0.00
	Metabolism of cofactors and vitamins							AlcF3P6.5	2.41	0.00
	Ubiquinone and other terpenoid_quinone biosynthesis	AlcF1P6.5	2.35	0.00	AlcF2P6.5	2.33	0.00	AlcF3P6.5	2.52	0.00
	Thiamine metabolism	AlcF1	2.13	0.04	AlcF2	2.08	0.00	AlcF3	2.29	0.00
	Retinol metabolism				AlcF2P6.5	2.06	0.00	AlcF3P6.5	2.20	0.00
	Riboflavin metabolism							AlcF3P6.5	2.31	0.00
	Folate biosynthesis							AlcF3	2.09	0.05
	Nicotinate and nicotinamide metabolism							AlcF3	2.06	0.05
	Pantothenate and CoA biosynthesis	AlcF1	2.29	0.00	AlcF2	2.37	0.00	AlcF3	2.45	0.00
Amino Acid Metabolism	Phenylalanine metabolism	AlcF1P6.5	2.19	0.00	AlcF2P6.5	2.32	0.00	AlcF3P6.5	2.66	0.00
	Lysine biosynthesis	AlcF1	2.56	0.00	AlcF2	2.57	0.00	AlcF3	2.69	0.00
	Valine_leucine and isoleucine biosynthesis	AlcF1P6.5	2.10	0.00	AlcF2P6.5	2.33	0.00	AlcF3	2.47	0.00
	Valine_leucine and isoleucine degradation	AlcF1	2.28	0.01	AlcF2	2.37	0.00	AlcF3P6.5	2.20	0.00
	Phenylalanine_tyrosine and tryptophan biosynthesis	AlcF1	2.46	0.01	AlcF2	2.39	0.00	AlcF3	2.62	0.00
	Aminoacidrelated enzymes	AlcF1	2.79	0.00	AlcF2	2.76	0.00	AlcF3	2.98	0.00
	Lysine degradation	AlcF1P6.5	2.31	0.01	AlcF2P6.5	2.21	0.00	AlcF3P6.5	2.37	0.01
	Tyrosine metabolism	AlcF1P6.5	2.07	0.01	AlcF2P6.5	2.11	0.00	AlcF3P6.5	2.28	0.01
	Cysteine and methionine metabolism				AlcF2	2.20	0.00	AlcF3	2.20	0.00
	Histidine metabolism							AlcF3	2.70	0.00
	Tryptophan metabolism							AlcF3P6.5	2.18	0.05
	Phenylpropanoid biosynthesis							AlcF3	2.43	0.00
Other Amino Acids	Glutathione metabolism	AlcF1P6.5	2.42	0.00	AlcF2P6.5	2.48	0.00	AlcF3P6.5	2.61	0.00
	Cyanoaminoacid metabolism	AlcF1P6.5	2.12	0.02				AlcF3	2.46	0.00
	D_Alanine metabolism							AlcF3	2.07	0.00
	Methane metabolism	AlcF1	2.64	0.01	AlcF2	2.62	0.00	AlcF3	2.76	0.00
	Sulfur metabolism	AlcF1P6.5	2.03	0.00	AlcF2P6.5	2.06	0.00	AlcF3P6.5	2.36	0.00

	Nitrogen metabolism	AlcF1P6.5	2.49	0.00	AlcF2P6.5	2.66	0.00	AlcF3P6.5	2.84	0.00
	Photosynthesis proteins	AlcF1	2.28	0.00	AlcF2	2.16	0.00	AlcF3	2.45	0.00
	Photosynthesis	AlcF1	2.29	0.00	AlcF2	2.16	0.00	AlcF3	2.46	0.00
	Oxidative phosphorylation							AlcF3	2.67	0.01
Glycan biosynthesis andMetabolism	Glycosyl transferases	AlcF1P6.5	2.31	0.01	AlcF2P6.5	2.42	0.00	AlcF3P6.5	2.52	0.00
	Lipopolysaccharide biosynthesis proteins	AlcF1P6.5	2.42	0.03	AlcF2P6.5	2.50	0.01	AlcF3P6.5	2.81	0.00
	Peptidoglycan biosynthesis	AlcF1	2.60	0.00	AlcF2	2.60	0.00	AlcF3	2.83	0.00
	Glycosaminoglyc and degradation	AlcF1P6.5	2.29	0.03	AlcF2P6.5	2.55	0.00			
	Otherglyc and degradation				AlcF2P6.5	2.87	0.00			
	Glycosphingolipid biosynthesis_ganglioseries				AlcF2P6.5	2.35	0.00			
	Lipopolysaccharide biosynthesis				AlcF2P6.5	2.28	0.01			
Biosynthesis of Other Secondary Metabolites	Penicillin andcephalosporin biosynthesis				AlcF2P6.5	2.03	0.00	AlcF3P6.5	2.08	0.00
	Biosynthesis andbio degradation of secondary metabolites	AlcF1P6.5	2.20	0.00						
	Butirosin and neomycin biosynthesis							AlcF3	2.22	0.00
Enzyme Families	Proteinkinases	AlcF1P6.5	2.27	0.05				AlcF3P6.5	2.50	0.00
	Peptidases	AlcF1	2.68	0.00	AlcF2	2.51	0.01	AlcF3	2.79	0.00
Carbohydrate Metabolism	Galactose metabolism	AlcF1P6.5	2.65	0.00	AlcF2P6.5	2.78	0.00	AlcF3P6.5	2.53	0.05
	Glyoxylate and dicarboxylate metabolism	AlcF1P6.5	2.35	0.00	AlcF2P6.5	2.45	0.00	AlcF3P6.5	2.80	0.00
	Fructose and mannose metabolism	AlcF1P6.5	2.40	0.02	AlcF2P6.5	2.63	0.00	AlcF3P6.5	2.85	0.00
	Starch and sucrose metabolism	AlcF1P6.5	2.66	0.00	AlcF2P6.5	2.41	0.00	AlcF3	2.40	0.01
	Pentose and glucuronate interconversions	AlcF1P6.5	2.70	0.00	AlcF2P6.5	2.79	0.00	AlcF3P6.5	2.96	0.00
	Ascorbate and aldarate metabolism	AlcF1P6.5	2.29	0.02	AlcF2P6.5	2.03	0.00	AlcF3P6.5	2.51	0.01
	Pyruvate metabolism				AlcF2P6.5	2.12	0.01	AlcF3P6.5	2.51	0.00
	Propanoate metabolism				AlcF2P6.5	2.23	0.04	AlcF3P6.5	2.60	0.00
	Pentose phosphate pathway				AlcF2P6.5	2.03	0.01	AlcF3P6.5	2.41	0.00
	Glycolysis_Gluconeogenesis							AlcF3P6.5	2.02	0.01
	Butanoate metabolism							AlcF3P6.5	2.43	0.00
	Inositolphosphate metabolism							AlcF3P6.5	2.37	0.00
	Biosynthesis and biodegradation of secondary metabolites							AlcF3P6.5	2.38	0.00
	Carbohydrate metabolism							AlcF3P6.5	2.65	0.00
	Glycan biosynthesis and metabolism							AlcF3P6.5	2.11	0.01

	Aminosugar and nucleotidesugar metabolism				AlcF2P6.5	2.51	0.00			
Lipid Metabolism	Fattyacid metabolism	AlcF1P6.5	2.29	0.03	AlcF2P6.5	2.33	0.00	AlcF3P6.5	2.56	0.00
	Biosynthesis of unsaturated fatty acids	AlcF1P6.5	2.18	0.01				AlcF3P6.5	2.37	0.00
	Fattyacid biosynthesis				AlcF2P6.5	2.02	0.00	AlcF3P6.5	2.19	0.03
	Glycerophospholipid metabolism				AlcF2	2.12	0.00	AlcF3	2.29	0.00
	Glycerolipid metabolism	AlcF1	2.23	0.00	AlcF2	2.31	0.00			
	Lipid biosynthesis proteins				AlcF2P6.5	2.03	0.00			
	Sphingolipid metabolism	AlcF1P6.5	2.36	0.04	AlcF2P6.5	2.58	0.00			
Xenobiotics Bio degradation and Metabolism	Drug metabolism_other enzymes	AlcF1	2.07	0.02	AlcF2	2.05	0.01	AlcF3	2.45	0.00
	Drug metabolism_cytochrome P450	AlcF1P6.5	2.01	0.00	AlcF2P6.5	2.10	0.00	AlcF3P6.5	2.21	0.00
	Metabolism of xenobiotics by cytochrome P450	AlcF1P6.5	2.02	0.00	AlcF2P6.5	2.08	0.00	AlcF3P6.5	2.21	0.00
	Benzoate degradation				AlcF2P6.5	2.06	0.04	AlcF3P6.5	2.50	0.00
	Caprolactam degradation	AlcF1P6.5	2.07	0.04				AlcF3P6.5	2.27	0.00
	Naphthalene degradation				AlcF2P6.5	2.03	0.00			
	Dioxin degradation							AlcF3P6.5	2.28	0.00
	Xylene degradation							AlcF3P6.5	2.20	0.00
	Toluene degradation							AlcF3P6.5	2.25	0.00
Nucleotide Metabolism	Pyrimidine metabolism	AlcF1	2.98	0.00	AlcF2	2.93	0.00	AlcF3	3.16	0.00
	Purine metabolism	AlcF1	2.78	0.00	AlcF2	2.65	0.00	AlcF3	2.85	0.01
Metabolism of Terpenoids and Polyketides	Prenyl transferases	AlcF1	2.20	0.01	AlcF2	2.15	0.01	AlcF3	2.43	0.00
	Terpenoid backbone biosynthesis	AlcF1	2.52	0.00	AlcF2	2.44	0.00	AlcF3	2.64	0.00
	Geraniol degradation	AlcF1P6.5	2.22	0.00	AlcF2P6.5	2.24	0.00	AlcF3P6.5	2.40	0.00
	Biosynthesis of siderophore group nonribosomal peptides	AlcF1P6.5	2.17	0.00	AlcF2P6.5	2.02	0.00	AlcF3P6.5	2.46	0.00
	Tetracycline biosynthesis							AlcF3P6.5	2.14	0.00

Supplementary table 3: Pathways modified in pectin treated mice based on fecal metabolomic analysis

Pathway Name	Nb of compounds included in the analysis	Total compounds in pathway	p	FDR	Impact
Inositol phosphate metabolism	2	28	0.000	0.000	0.11163
Ascorbate and aldarate metabolism	3	9	0.000	0.000	0.4
Starch and sucrose metabolism	5	19	0.000	0.000	0.24448
Methane metabolism	2	9	0.000	0.000	0.4
Cyanoamino acid metabolism	2	6	0.000	0.000	0
Lysine biosynthesis	1	4	0.000	0.000	0
Lysine degradation	1	23	0.000	0.000	0
Biotin metabolism	1	5	0.000	0.000	0
Purine metabolism	13	68	0.000	0.000	0.14028
Tyrosine metabolism	3	44	0.000	0.000	0.14045
Valine, leucine and isoleucine degradation	5	38	0.000	0.000	0.0238
Porphyrin and chlorophyll metabolism	2	27	0.000	0.000	0
Pentose and glucuronate interconversions	5	16	0.000	0.000	0.26666
Valine, leucine and isoleucine biosynthesis	6	11	0.000	0.000	0.99999
Histidine metabolism	3	15	0.000	0.000	0.24194
Glyoxylate and dicarboxylate metabolism	2	18	0.000	0.000	0.32258
Citrate cycle (TCA cycle)	5	20	0.000	0.000	0.24593
D-Glutamine and D-glutamate metabolism	3	5	0.000	0.000	1
Nitrogen metabolism	4	9	0.000	0.000	0
Linoleic acid metabolism	1	16	0.000	0.000	1
Pantothenate and CoA biosynthesis	5	15	0.000	0.001	0.02041
Cysteine and methionine metabolism	4	27	0.000	0.001	0.1351
Aminoacyl-tRNA biosynthesis	18	69	0.000	0.001	0.12903
Glutathione metabolism	6	26	0.000	0.001	0.09828
beta-Alanine metabolism	4	17	0.000	0.001	0.44444
Butanoate metabolism	6	22	0.000	0.001	0.02899

Alanine, aspartate and glutamate metabolism	10	24	0.000	0.001	0.78269
Glycine, serine and threonine metabolism	10	31	0.000	0.001	0.59903
Ubiquinone and other terpenoid-quinone biosynthesis	1	3	0.001	0.001	0
Primary bile acid biosynthesis	5	46	0.001	0.001	0.12626
Sphingolipid metabolism	2	21	0.001	0.001	0.01504
Phenylalanine, tyrosine and tryptophan biosynthesis	2	4	0.001	0.002	1
Phenylalanine metabolism	2	11	0.001	0.002	0.40741
Steroid biosynthesis	1	35	0.002	0.002	0.05394
Steroid hormone biosynthesis	1	72	0.002	0.002	0.01689
Pyrimidine metabolism	5	41	0.002	0.003	0.08292
Galactose metabolism	6	26	0.002	0.003	0.07627
Arginine and proline metabolism	14	44	0.003	0.004	0.54477
Taurine and hypotaurine metabolism	3	8	0.003	0.004	0.71428
Selenoamino acid metabolism	1	15	0.004	0.005	0
Pyruvate metabolism	2	23	0.004	0.006	0.18375
Propanoate metabolism	2	20	0.006	0.007	0
Fatty acid elongation in mitochondria	1	27	0.008	0.010	0
Fatty acid metabolism	1	39	0.008	0.010	0
Glycerolipid metabolism	3	18	0.010	0.013	0.41129
Pentose phosphate pathway	4	19	0.018	0.021	0.41291
Glycolysis or Gluconeogenesis	3	26	0.018	0.021	0.13406
Biosynthesis of unsaturated fatty acids	7	42	0.020	0.023	0
Nicotinate and nicotinamide metabolism	2	13	0.034	0.038	0.2381
Fatty acid biosynthesis	4	43	0.035	0.038	0
Tryptophan metabolism	2	40	0.041	0.044	0.28702
Glycerophospholipid metabolism	5	30	0.046	0.048	0.11297
Amino sugar and nucleotide sugar metabolism	2	37	0.144	0.147	0.08988
Arachidonic acid metabolism	1	36	0.384	0.384	0.32601

FDR: false discovery rate

Supplementary table 4: Clinical characteristics of alcoholic patients for tryptophan pathway analysis.

	Alcoholic patients without alcoholic hepatitis (noAH) (n=15)	**Alcoholic patients with severe alcoholic hepatitis (sAH)** (n=14)
Age (years)	52.07 ± 8.21	55.79 ± 12.4
Sex (male,%)	10 (67)	13 (93)
BMI (kg/m2)	22.08 ± 4.3	25.56 ± 5.05
Alcohol (g/day)*	149.14 ± 101.81	77.86 ± 36.2
Alcohol duration (years)	15.04 ± 12.31	21.23 ± 10.37
Smoking (yes,%)	11 (73)	9 (64)
AST (IU/L)**	38.93 ± 20.83	131.36 ± 105.03
ALT (IU/L)	36.27 ± 16.18	42.5 ± 16.58
Bilirubin**	13.13 ± 7.72	229 ± 221.84
GGT (IU/L)*	121.73 ± 97.53	423.43 ± 384.51
Platelets (×10^9/L) *	211.93 ± 72.48	127 ± 114.12
PT (%)***	98.67 ± 4.13	39 ± 14.46
MELD score***	2.78 ± 2.92	22.84 ± 7.5

BMI: body mass index, AST: aspartate transaminase, ALT: alanine transaminase, GGT: gamma-glutamyltransferase, PT: prothrombin time, MELD: Model for End-Stage Liver Disease. *<0.05, **<0.01, ***<0.001. Data are presented as mean ± SD.

Supplementary table 5: Primer sequences used for q-PCR reactions

Name	5'- Forward - 3'	5'- Reverse - 3'
18s	GTAACCCGTTGAACCCCATT	CCATCCAATCGGTAGTAGCG
ahrr	ACATACGCCGGTAGGAAGAGA	GGTCCAGCTCTGTATTGAGGC
ccl2	AGGTCCCTGTCATGCTTCTG	TCTGGACCCATTCCTTCTTG
ccl3	*purchased from Qiagen , ref QT00248199*	
cyp1a1	CAGGATGTGTCTGGTTACTTTGAC	CTGGGCTACACAAGACTCTGTCTC
gapdh	GTGGACCTCATGGCCTACAT	TGTGAGGGAGATGCTCAGTG
il1β	AAGGTCCACGGGAAAGACAC	AGCTTCAGGCAGGCAGTATC
il17	TTTAACTCCCTTGGCGCAAAA	CTTTCCCTCCGCATTGACAC
il22	ATGAGTTTTTCCCTTATGGGGAC	GCTGGAAGTTGGACACCTCAA
reg3β	GGCAACTTCACCTCACAT	TGGGAATGGAGTAACAATG
reg3γ	CAAGATGTCCTGAGGGC	CCATCTTCACGTAGCAGC
scd1	CCGGAGACCCTTAGATCGA	TAGCCTGTAAAAGATTTCTGCAAA
tgfβ	GCAACATGTGGAACTCTACCAGAA	GACGTCAAAAGACAGCCACTCA
tnfα	TGGGAGTAGACAAGGTACAACCC	CATCTTCTCAAAATTCGAGTGACAA